

A chemical probe to modulate human GID4 Pro/N-degron interactions

Received: 17 January 2023

Accepted: 12 April 2024

Published online: 21 May 2024

 Check for updates

Dominic D. G. Owens  ^{1,14}, Matthew E. R. Maitland ^{1,2,3,4,14}, Aliakbar Khalili Yazdi ¹, Xiaosheng Song  ¹, Viviane Reber  ⁵, Martin P. Schwalm  ^{6,7}, Raquel A. C. Machado  ¹, Nicolas Bauer  ^{6,7}, Xu Wang ², Magdalena M. Szewczyk ¹, Cheng Dong  ¹, Aiping Dong ¹, Peter Loppnau ¹, Matthew F. Calabrese  ⁸, Matthew S. Dowling ⁸, Jisun Lee  ⁸, Justin I. Montgomery ⁸, Thomas N. O'Connell ⁸, Chakrapani Subramanyam ⁸, Feng Wang ⁸, Ella C. Adamson ¹, Matthieu Schapira  ^{1,9}, Matthias Gstaiger  ⁵, Stefan Knapp  ^{6,7}, Masoud Vedadi ^{1,9}, Jinrong Min  ^{1,10,11}, Gilles A. Lajoie ^{3,4}, Dalia Barsyte-Lovejoy  ^{1,9}, Dafydd R. Owen  ⁸, Caroline Schild-Poulter  ^{2,3} & Cheryl H. Arrowsmith  ^{1,12,13} 

The C-terminal to LisH (CTLH) complex is a ubiquitin ligase complex that recognizes substrates with Pro/N-degrons via its substrate receptor Glucose-Induced Degradation 4 (GID4), but its function and substrates in humans remain unclear. Here, we report PFI-7, a potent, selective and cell-active chemical probe that antagonizes Pro/N-degron binding to human GID4. Use of PFI-7 in proximity-dependent biotinylation and quantitative proteomics enabled the identification of GID4 interactors and GID4-regulated proteins. GID4 interactors are enriched for nucleolar proteins, including the Pro/N-degron-containing RNA helicases DDX21 and DDX50. We also identified a distinct subset of proteins whose cellular levels are regulated by GID4 including HMGCS1, a Pro/N-degron-containing metabolic enzyme. These data reveal human GID4 Pro/N-degron targets regulated through a combination of degradative and nondegradative functions. Going forward, PFI-7 will be a valuable research tool for investigating CTLH complex biology and facilitating development of targeted protein degradation strategies that highjack CTLH E3 ligase activity.

The half-life or stability of most intracellular proteins is governed by the presence of short linear sequences known as degrons^{1–4}. Degrongs at the N or C terminus of a protein, known as N and C degrons, or internal degrons such as PEST sequences, recruit distinct E3 ubiquitin ligases to polyubiquitylate substrates and target them for proteasomal degradation^{1,5}. E3 ligase-mediated polyubiquitylation of proteins via ubiquitin Lysine (K)-48 chains or K48-K11 branched chains typically leads to substrates being targeted to the 26S proteasome for subsequent degradation⁶. Degrongs may be recognized by E3 ligases directly or may undergo processing such as proteolytic trimming by aminopeptidases,

addition of terminal amino acids or other posttranslational modifications including phosphorylation^{1–4}. Degradation of proteins with distinct degrons occurs at different rates depending on the specific downstream enzymatic machinery recruited by each degron^{2,7}. Collectively, degron sequences fine-tune the abundance of intracellular proteins and further insights into degron recognition pathways will likely inform therapeutic efforts that use targeted protein degradation⁸.

The Pro/N-degron pathway is a recently identified pathway that recognizes N-terminal degrons containing unmodified Proline residues (Pro/N-degrons), either at position one or two of the sequence^{9–11}.

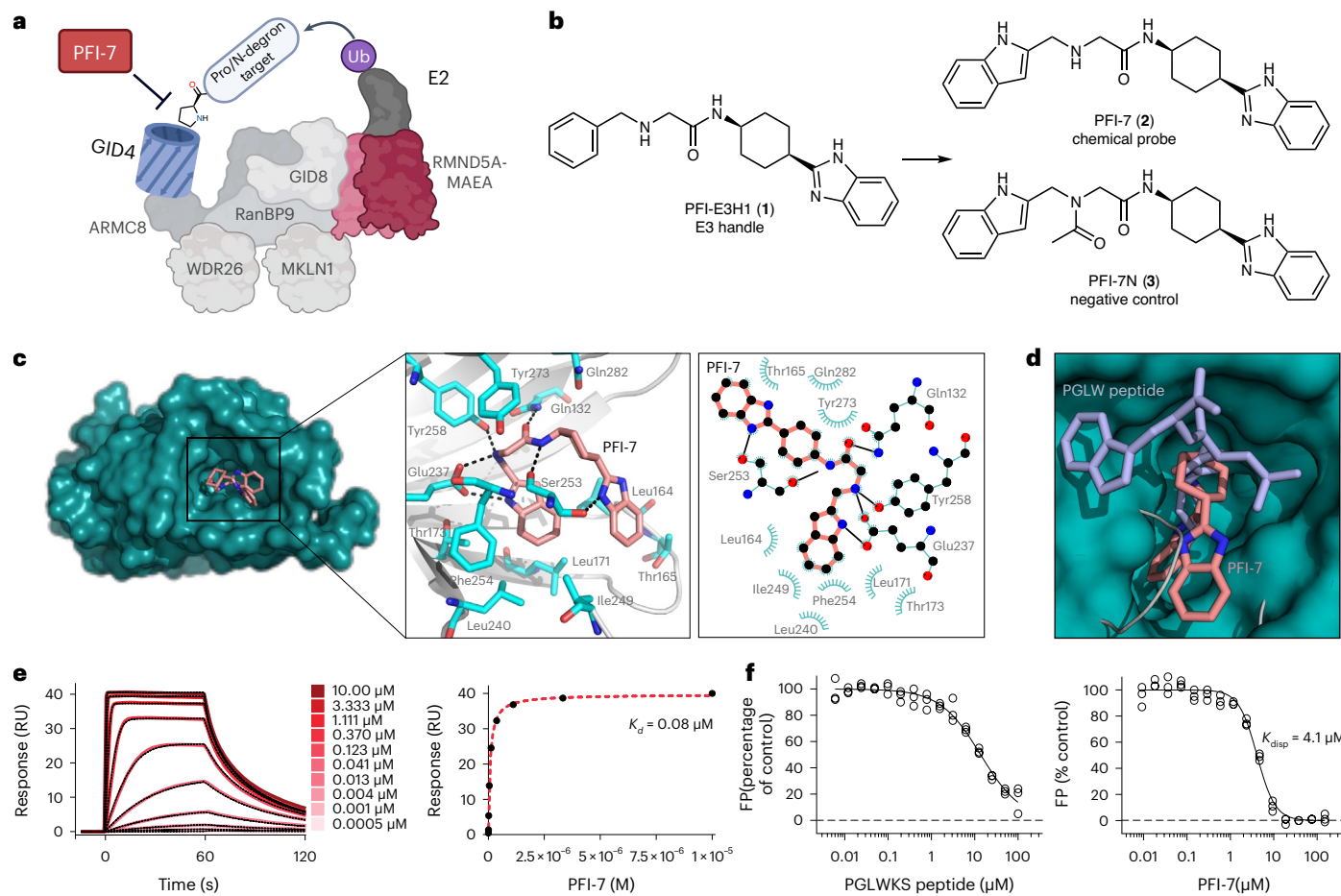


Fig. 1 | PFI-7 binds in the substrate binding pocket of human GID4.

a, Schematic of GID4 bound to the human CTLH complex with E2 enzyme and ubiquitin shown. The recognition of degron-containing substrates by GID4 is inhibited by GID4 antagonist PFI-7. Created with BioRender.com. **b**, Chemical structures of PFI-E3H1 (GID4 E3 handle), PFI-7 (GID4 chemical probe) and PFI-7N (negative control for PFI-7). **c**, Crystal structure (left panel) of PFI-7 (shown in pink) bound to GID4 (shown in gray and teal) (PDB 7SLZ). The right panel shows in two dimensions the key interactions between GID4 and PFI-7. Hydrogen bonds are black dashed lines (left panel) or solid lines (right panel). **d**, Superimposed image of the PFI-7 (pink) and GID4 (teal surface) cocrystal structure with the previously determined (PDB 6CDC) cocrystal structure of Pro/N-degron peptide (light blue) with GID4 (gray ribbon). **e**, SPR analysis of the binding of PFI-7 to GID4 in which solutions of serially diluted compounds flowed over immobilized

GID4 and the resulting response unit (RU) signals were monitored. Left, a representative sensorgram for each compound is shown (solid red lines) with the corresponding 1:1 binding model kinetics fit indicated (dashed black lines). Right, the steady state response obtained from the data (left) is indicated (black circles) along with the corresponding steady state 1:1 binding model fitting (dashed red lines). Experiments were performed in triplicate ($n = 3$). **f**, Fluorescence polarization (FP)-based peptide displacement assay. Compounds were tested for competing with the fluorescein-labeled PGLWKS peptide for binding to GID4. Left, unlabeled PGLWKS peptide was used as a control (0.006 to 100 μ M). Right, PFI-7 was used at concentrations ranging from 0.01 to 150 μ M. All experiments were performed in triplicate ($n = 3$) and the calculated K_{disp} value is indicated.

The Pro/N-degron pathway in *Saccharomyces cerevisiae* allows cells to quickly adapt their metabolism and maintain homeostasis^{9,12}. Pro/N-degron-containing gluconeogenic enzymes are recognized by the Gid4 β -barrel substrate binding pocket and subsequently ubiquitylated by a multisubunit E3 ligase complex called the GID complex, targeting them for proteasomal degradation⁹. Many of the orthologous GID complex subunits exhibit conserved sequence homology and function between yeast and humans, but as several subunits contain a CTLH domain, the complex is commonly referred to as the CTLH complex in humans (Fig. 1a)¹³. Notable differences between the yeast and human complexes have been observed¹⁴. In *S. cerevisiae*, Gid4 is interchangeable with other substrate receptors including Gid10 and Gid11 (refs. 15–17), while GID4 is thus far the only CTLH complex substrate receptor identified in humans, despite some substrates being degraded in a GID4 independent manner¹⁸. In humans, the CTLH complex is implicated in a wide variety of cellular processes including autophagy, development, cell cycle regulation and primary cilium function¹⁴. Mutations in, and overexpression of, CTLH complex members are also common in some

cancers¹⁹. Mutations in the substrate binding pocket of GID4 that are likely to disrupt substrate binding have been reported in glioma, breast and pancreatic carcinoma samples¹¹. Together, this suggests that the role of the CTLH complex in humans has expanded beyond the initial function evolved in yeast, possibly through acquisition of a wider set of ubiquitylation substrates.

Substrates of the CTLH complex have been more challenging to identify in humans than in yeast. The first human CTLH substrate to be identified was HMG box protein 1 (HBP1)²⁰, a transcription factor responsible for inhibiting expression of proproliferative cell cycle regulators. HBP1 is ubiquitylated and degraded independently of GID4 (refs. 18,20), suggesting degradation is mediated via an alternative recognition subunit in CTLH other than GID4. Since then, a handful more degradative substrates of the complex have been suggested including BICC1 (ref. 21), MKLN1 (ref. 22), LMNB2 (ref. 23), RAF1 (ref. 24) and ZMYND19 (ref. 18). Ubiquitylation of glycolysis enzymes PKM2 and LDHA is dependent on the CTLH complex²⁵, indicating a conserved role for the GID–CTLH complex in regulating metabolism in yeast and

humans. However, ubiquitylation of PKM2 and LDHA does not result in their degradation, instead it reduces their activity to decrease glycolytic metabolism²⁵. None of the human CTLH complex substrates characterized so far contain either a canonical Pro/N-degron, or the more flexible degron sequences that were recently determined to also be recognized by GID4 *in vitro*^{26,27}. Bioinformatic prediction has been used to identify potential substrates based on the presence of a canonical Pro/N-degron consensus sequence¹¹, and some of these putative substrates have been shown to interact with the CTLH complex²⁸; however, a global assessment of GID4-dependent interactors of the CTLH complex and the role GID4 plays in proteome regulation in humans is so far lacking.

To address this knowledge deficit, we developed a selective antagonist of human GID4. PFI-7 is a chemical probe that binds within the β-barrel of GID4 substrate binding pocket, disrupting its interaction with the canonical Pro/N-degron peptide in cells. Using proximity-dependent biotinylation (BioID2-GID4) coupled with liquid chromatography with tandem mass spectrometry (LC-MS/MS), we identify dozens of endogenous GID4 interactors whose interaction with GID4 is reduced by PFI-7. GID4-dependent interactors are enriched for nucleolar proteins and proteins associated with RNA metabolism including RNA helicases. A subset of interactors exhibit canonical Pro/N-degrons, while most do not, implicating versatility in substrate recruitment to the CTLH complex by GID4. GID4-regulated abundances of proteins included RNA helicases and the mevalonate precursor enzyme HMGCS1, while levels of several GID4 interactors did not change after GID4 inhibition, showing that recruitment to GID4 via Pro/N-degron sequences is not always sufficient to promote proteasomal degradation. This proteome-wide assessment sheds new light on GID4-mediated CTLH complex interactors and identifies proteins regulated by GID4–CTLH. Furthermore, this work positions PFI-7 as an important research tool to further dissect mechanistic details and biological roles of the CTLH complex in health and disease. Our data also provide insights into proteome regulation by CTLH–GID4 that will inform future efforts to establish GID4 recruitment reagents or drugs for targeted protein degradation^{8,29}.

Results

Discovery of a potent ligand targeting GID4

To discover a chemical probe to explore the E3 ligase activity of the CTLH complex, we targeted its evolutionarily conserved substrate receptor, GID4 (Fig. 1a). Affinity selection mass spectrometry and subsequent medicinal chemistry optimization led to the discovery of the moderately potent ‘E3 handle’ compound, PFI-E3H1 (**1**) (Fig. 1b)³⁰. After slight modification to the PFI-E3H1 scaffold to improve anticipated potency, the compound PFI-7 (**2**) and its negative control analog (modified with an acetyl group on the critical secondary amine), PFI-7N (**3**), were selected for further characterization (Fig. 1b). A cocrystal structure shows PFI-7 bound deep within the GID4 Pro/N-degron

peptide binding pocket partially occupying the peptide binding site¹¹ (Fig. 1c,d, Supplementary Table 1 and Supplementary Fig. 1). PFI-7 binds through a network of hydrophobic and H-bond interactions (Fig. 1c), with the benzimidazole moiety surface exposed, indicating a site on PFI-7 that will likely tolerate derivatization. PFI-7 also displaces a loop that mediates a hydrogen bond between G251 of GID4 and the backbone amide of the fourth residue of the degron peptide¹¹ (Fig. 1d). PFI-7 binds to GID4 with a K_d of 79 ± 7 nM, as determined by surface plasmon resonance (SPR) (Fig. 1e). Furthermore, PFI-7 can directly displace the Pro/N-degron peptide PGLWKS from the GID4-binding pocket in a peptide displacement assay (Fig. 1f, $K_{\text{disp}} = 4.1 \pm 0.2$ μM). Together this biophysical characterization clearly demonstrates that PFI-7 binds to the GID4 substrate binding pocket and disrupts Pro/N-degron binding.

PFI-7 is a selective and potent GID4 antagonist in cells

To profile target engagement in a cellular context and quantify the extent to which PFI-7 engages and antagonizes GID4 in live cells, we used NanoLuciferase (NanoLuc) bioluminescence resonance energy transfer (NanoBRET) protein–protein interaction (PPI) assays. In this assay, NanoLuc protein that acts as an energy donor was N-terminally tagged with PGLWKS peptide to mimic an endogenous Pro/N-degron (Fig. 2a). GID4 was C-terminally tagged with haloalkane dehalogenase (HaloTag) that irreversibly binds to a cell-permeable chloroalkane-modified 618 nm fluorophore, the BRET energy acceptor. A dose-dependent decrease in GID4-HaloTag binding to PGLWKS-NanoLuc was observed on treatment of human embryonic kidney 293T (HEK293T) cells with PFI-7 (half-maximum inhibitory concentration (IC_{50}) of 0.54 ± 0.13 μM) (Fig. 2b), but not with PFI-7N, thus indicating that PFI-7 inhibits Pro/N-degron binding by GID4 in live cells. In a complementary assay configuration, we developed a tracer compound consisting of a derivatized PFI-E3H1 conjugated to a 590 nm fluorophore (GID4-tracer (**4**)) that dose-dependently bound to NanoLuc-tagged GID4 in live cells (Fig. 2c–e). PFI-7 effectively competed with the GID4-NanoLuc and GID4-tracer interaction in a dose-dependent manner (GID4-N $IC_{50} = 0.35 \pm 0.07$ μM, GID4-C $IC_{50} = 0.28 \pm 0.05$ μM) (Fig. 2f).

To profile ligand selectivity in a cellular context, we synthesized NB716 (**5**), a biotinylated derivative of PFI-E3H1. We applied NB716 to whole-cell extracts from HeLa cells that expressed a BioID2-GID4 fusion protein (used in the experiments below) and then enriched NB716-bound proteins via streptavidin-coated beads (Fig. 2g). Using label-free proteomics, GID4 was detected as one of the most highly enriched NB716-bound proteins while other significantly enriched proteins included GID4 direct binder ARMC8 (ref. 31) (Fig. 1a) and other members of the CTLH complex, suggesting that GID4 was pulled down in native complexes (Extended Data Fig. 1 and Supplementary Data). Only GID4 was significantly depleted by competition with PFI-7, whereas the enrichment profile was not appreciably altered by PFI-7N (Fig. 2h and Supplementary Data). Additionally, there were minimal cytotoxic effects following treatment of a panel of cell lines with PFI-7

Fig. 2 | PFI-7 cellular target engagement and selectivity. **a**, NanoBRET PPI assay to quantify inhibition of GID4 Pro/N-degron binding by PFI-7. Schematic of PGLWKS degron-tagged NanoLuciferase (NanoLuc, donor) and C-terminally tagged GID4-haloalkane dehalogenase (HaloTag, HT) irreversibly bound to a cell-permeable 618 nm fluorochrome (HaloLigand, HL, acceptor). Created with BioRender.com. **b**, BRET ratio as a percentage of vehicle (DMSO) control in cells treated with increasing concentrations of PFI-7 or PFI-7N. Data are from three independent experiments ($n = 3$). **c**, NanoBRET target engagement assay using GID4-tracer compound. Left, schematic of GID4-NanoLuc fusion protein (donor) and a GID4-tracer compound consisting of a GID4-binding moiety related to PFI-E3H1 derivatized with a 590 nm fluorophore (acceptor). Created with BioRender.com. **d**, Right, chemical structure of GID4-tracer compound. **e**, Titration of GID4-tracer compound binding to N- or C-terminally NanoLuc-tagged GID4. BRET ratio is shown as a percentage of the highest measured value. Data are from two independent experiments ($n = 2$). **f**, Competition of GID4-tracer compound

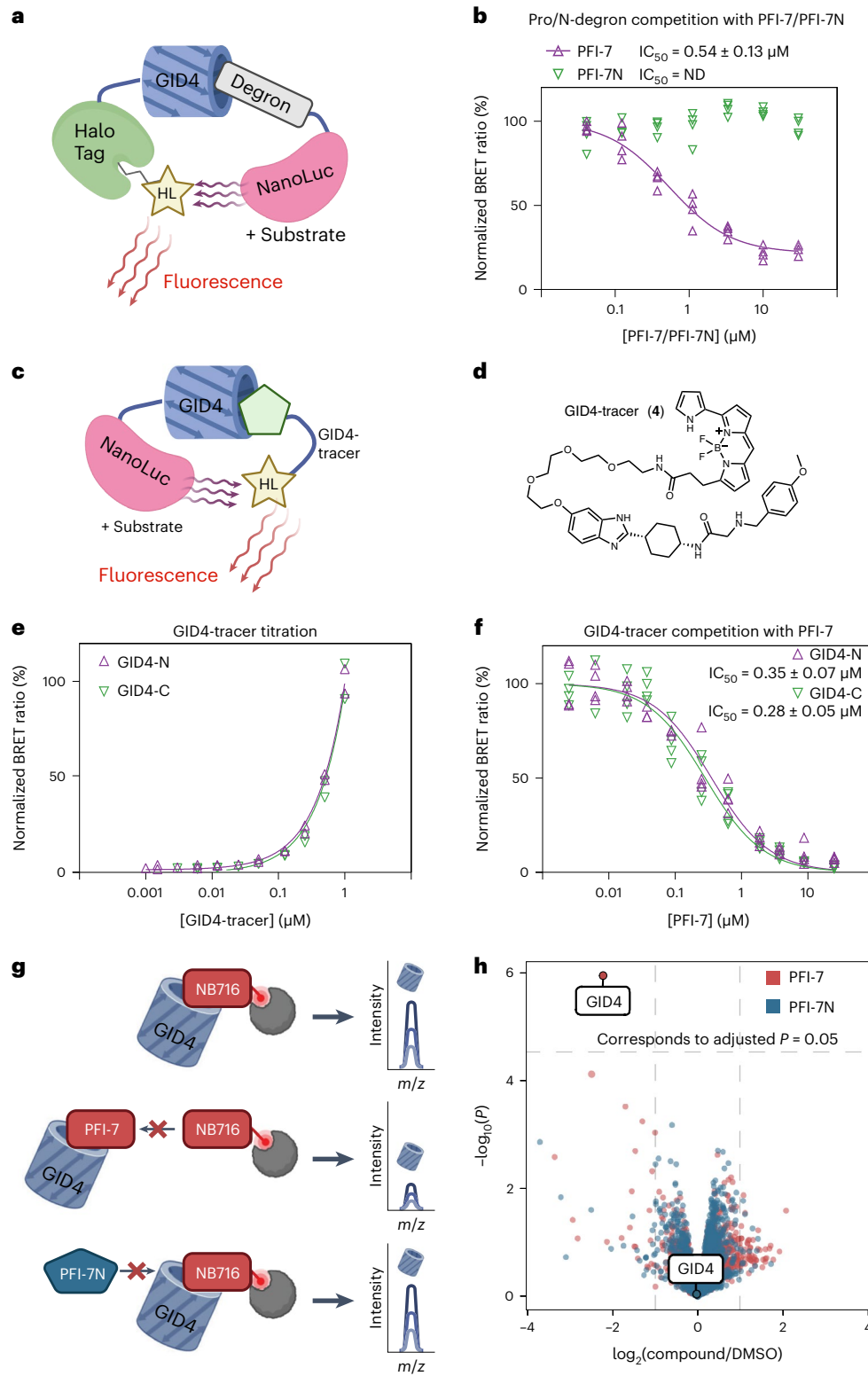
binding to N- or C-terminally NanoLuc-tagged GID4 using GID4 antagonist PFI-7. BRET ratio is shown as a percentage of vehicle (DMSO) treated cells. Data are from two independent experiments ($n = 2$). **g**, A chemoproteomics approach is used to assess specificity of PFI-7. We used NB716, a biotinylated PFI-E3H1 analog, to purify proteins interacting with PFI-7. When the nonbiotinylated-GID4 inhibitor PFI-7 is added in excess, target binding site is occupied and GID4 can therefore no longer bind NB716 resulting in lower protein intensities as measured by mass spectrometry. Addition of a nonbinder control such as PFI-7N has no effect on the intensity of PFI-7 target proteins. Created with BioRender.com. **h**, Proteomic profiling of NB716 pulldown when in competition with PFI-7 (red dots) and PFI-7N (blue dots). The differential abundance was calculated and significance was determined across the triplicates using a two-tailed moderated t-test with multiple testing correction using the Benjamini–Hochberg method. $n = 3$ independent experiments. ND, no data.

or PFI-E3H1 up to 10 μ M over 3 days (Extended Data Fig. 2). Together, these data show that PFI-7 selectively engages GID4 in live cells to inhibit Pro/N-degron binding and is a suitable tool compound for use in cellular studies to interrogate GID4-mediated recruitment to the CTLH complex.

GID4 interacts with nucleolar and RNA splicing proteins

The interactome of GID4 has never been determined using GID4 as a bait. Thus, to elucidate the GID4 interactome, proximity-dependent

biotinylation was performed followed by protein identification by LC–MS/MS (Fig. 3a). The GID4 fusion protein (hemagglutinin (HA)-myc-BioID2-GID4, hereafter referred to as BioID2-GID4) preserves the GID4 C-terminal anchor required for CTLH complex binding via ARMC8 α (ref. 31) (Extended Data Fig. 3a). BioID2-GID4 was functional as it interacted with the endogenous CTLH complex by coimmunoprecipitation (Extended Data Fig. 3b). On doxycycline induction, BioID2-GID4 elicited biotinylation of proteins in an exogenous biotin-dependent manner (Extended Data Fig. 3c). BioID2-GID4 showed similar localization



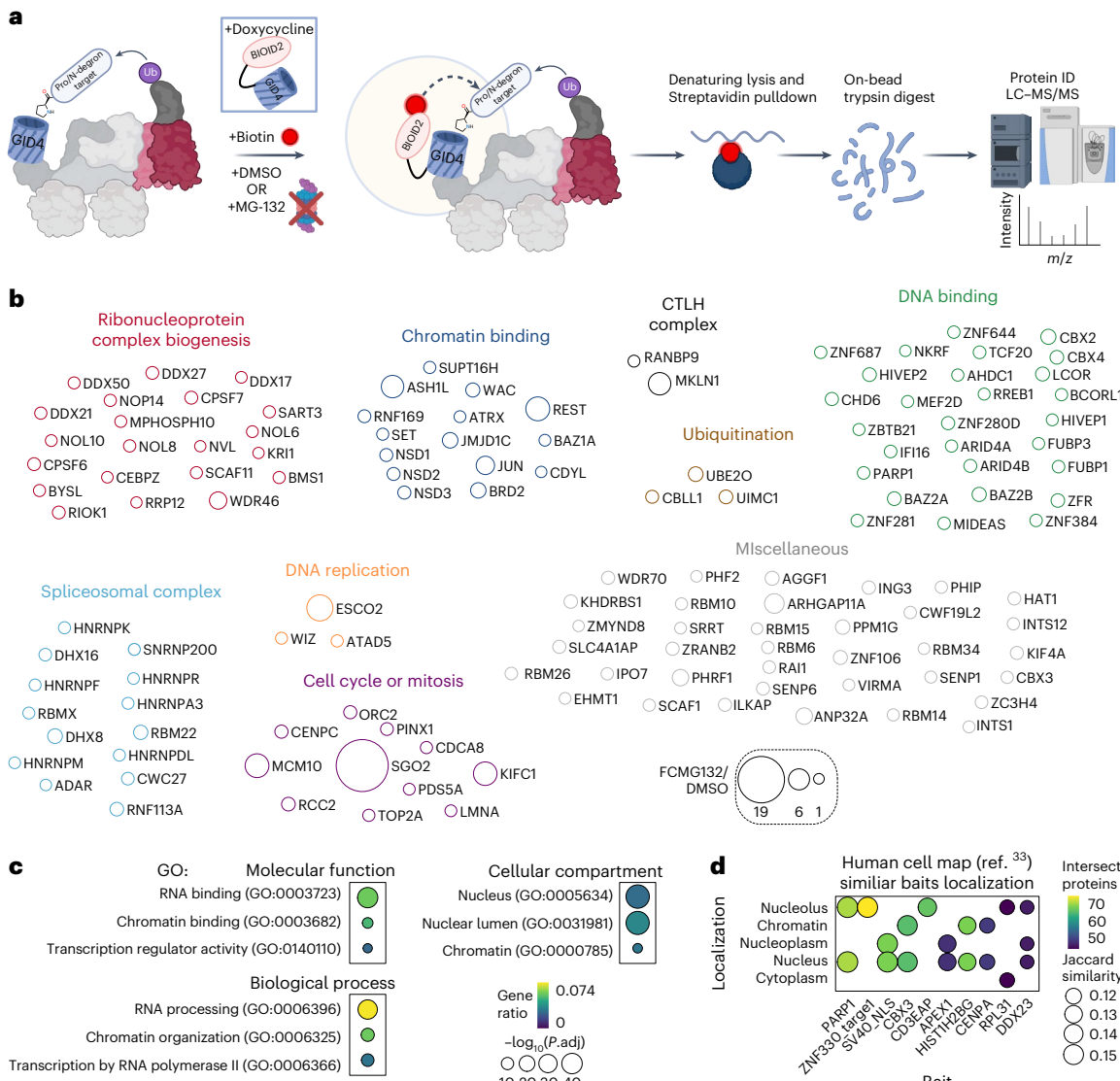


Fig. 3 | GID4-BioID2 in the presence and absence of proteasome inhibition.

a, Schematic of GID4 proximity-dependent biotinylation workflow. Doxycycline-inducible BioID2-GID4 is expressed for 24 h in the presence or absence of MG132. On induction, BioID2-GID4 binds to the endogenous CTLH complex and biotinylates proximal interacting proteins. Biotinylated proteins are enriched before protein identification using LC-MS/MS. Created with BioRender.com. **b**, Top 133 GID4 interactors (SP > 0.9, spectral counts > 5) classified by functional annotation. The size of each circle represents fold change between MG132 and DMSO-treated samples. Larger circles contained more spectral counts in MG132. Data are from CPMG132/DMSO.

three independent experiments ($n = 3$, BioID2 + MG132) or four independent experiments ($n = 4$, BioID2 + DMSO, BioID2-GID4 + DMSO, BioID2-GID4 + MG132). **c**, Gene ontology (GO) terms functional annotation of GID4 interactors (SP > 0.9). Gene ratio represents the fraction of genes in each gene ontology category that were identified. The enrichment analysis was performed with the goseq package in R, using a two-sided Wallenius noncentral hypergeometric test and *P* values were adjusted using the Benjamini–Hochberg method. **d**, Top ten most similar baits to GID4 found in the human cell map database. Jaccard similarity represents the percentage overlap between sets of interacting proteins.

to HA-GID4 as measured by immunofluorescence and western blot (Extended Data Fig. 3d,e and ref. 22). To interrogate the transient GID4 interactors that are degraded on ubiquitylation by the CTLH complex, the GID4 interactome was analyzed in the presence and absence of proteasome inhibitor MG132, as has been done to identify SCF(β-TrCP1/2) substrates³². Samples segregated based on GID4 expression in uniform manifold approximation and projection (UMAP) analysis, while proteasome inhibitor contributed little to sample clustering (Extended Data Fig. 3f). Using a high-confidence threshold, 196 proteins were significantly enriched in BioID2-GID4 samples compared to BioID2 alone (Saint probability (SP) ≥ 0.9 , Fig. 3b and Supplementary Data). Two members of the CTLH complex were identified as GID4 interactors, RANBP9 and MKLN1 (Fig. 3b and Extended Data Fig. 3g). Twenty of the high-confidence GID4 interactors have previously been described as interactors of the CTLH complex in the BioGRID database²⁸ including

DDX50 (Extended Data Fig. 3h). GID4 interactors were associated with ribonucleoprotein complex biogenesis, chromatin binding, DNA binding and spliceosomal complex, as well as ubiquitination and mitosis (Fig. 3b). GID4 interactors were significantly enriched for gene ontology terms associated with ribosomal RNA binding and processing, chromatin binding and organization, and the nucleus and nuclear lumen cellular compartments (Fig. 3c). The GID4 interactome shares most similarity with the previously identified interactomes³³ of other proteins localized to the nucleolus, nucleus, nucleoplasm and chromatin (Fig. 3d). Taken together, GID4 interacts broadly with distinct classes of nuclear proteins involved in RNA processing, chromatin, splicing and transcription.

RNA helicases DDX21 and DDX50 interact with GID4

Since human substrates of the Pro/N-degron pathway have remained elusive, we determined the GID4 interactors that specifically

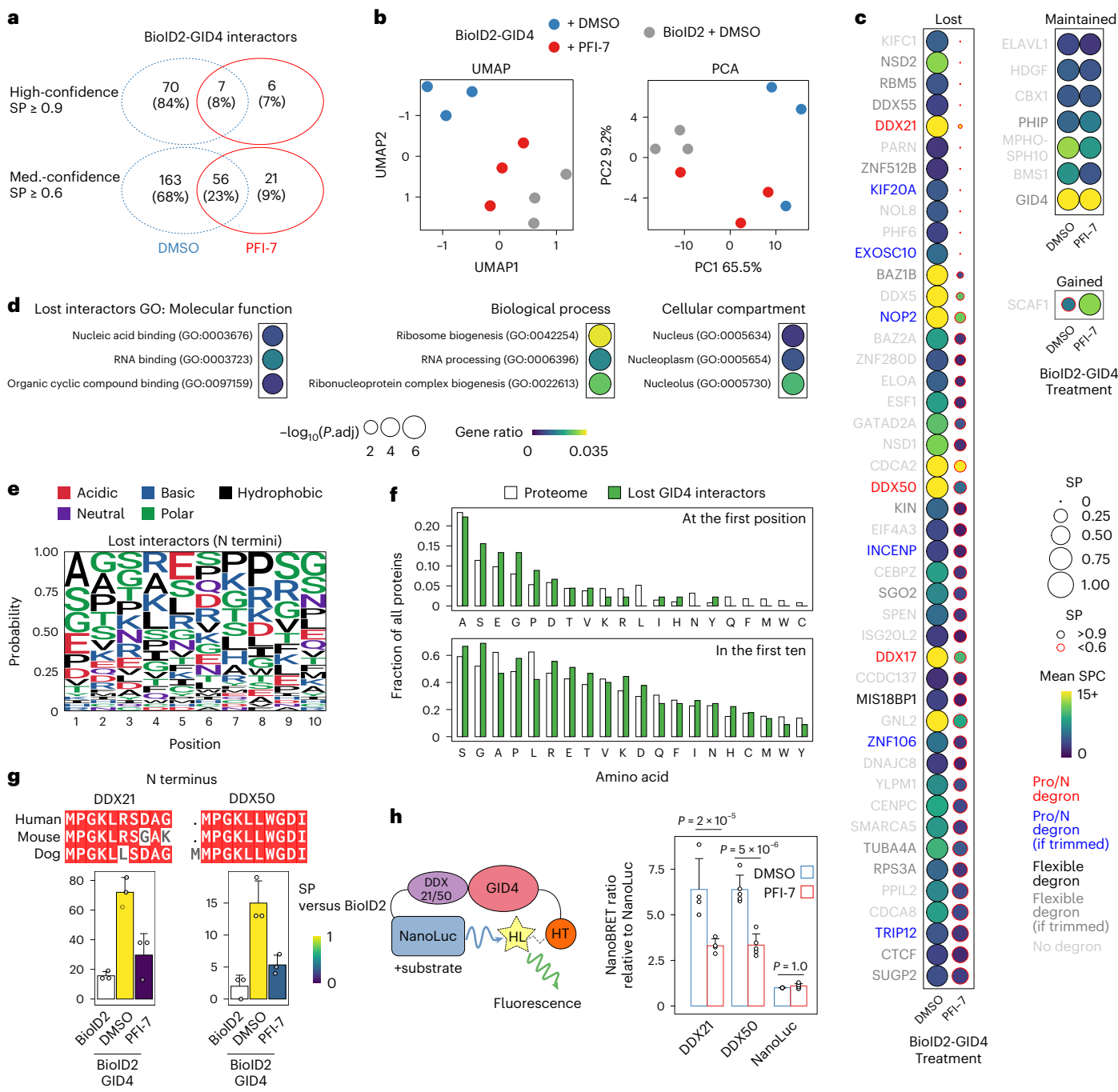


Fig. 4 | GID4-BioID2 in the presence and absence of PFI-7. **a**, Numbers of BioID2-GID4 interacting proteins identified in DMSO and PFI-7 treated samples. Data in this figure are from three independent experiments ($n = 3$). **b**, Clustering of log₂-normalized area intensities by UMAP and PCA. PCA was done on all proteins with SP > 0.6 in BioID2-GID4 condition (217 proteins). UMAP was done on proteins with SP > 0.6 in BioID2-GID4 and a difference in SP > 0.9 between BioID2-GID4 and BioID2-GID4 + PFI-7 (11 proteins). **c**, GID4 interactors that were lost (DMSO SP > 0.9, PFI-7 SP < 0.6), maintained (DMSO SP > 0.9, PFI-7 SP > 0.9) and gained (DMSO SP < 0.6, PFI-7 SP > 0.9) are shown. Pro/N-degron, N-terminal Pro followed by one of (S/H/T/A); flexible Pro/N-degron, hydrophobic amino acid (P/I/L/F/V) followed by a small side-chain residue (S/T/G/V/A); if trimmed, degron appeared within the first ten amino acids. **d**, GO terms functional annotation of GID4 interactors that were lost (DMSO SP > 0.9, PFI-7 SP < 0.6). Gene ratio represents the fraction of genes in each gene ontology category that were identified. The enrichment analysis was performed with the goseq package in R, using a two-sided Wallenius noncentral hypergeometric test and P values were adjusted using the Benjamini–Hochberg method. **e**, Consensus sequence of ten

N-terminal amino acids of GID4 interactors that were lost after PFI-7 treatment. **f**, Enrichment of different N-terminal amino acids at the first position or within the first ten amino acids of GID4 interactors that were lost after PFI-7 treatment and the background in the proteome. χ^2 tests d.f. = 19, $P = 0.766$ (enrichments at first position), $P = 0.632$ (enrichments in the first ten). **g**, N-terminal sequence conservation of DDX21 and DDX50 is shown. Spectral counts and SP are shown for GID4-BioID2 versus BioID2 for DMSO and PFI-7-treated samples. Error bars indicate standard deviation. **h**, Schematic of DDX21/50 GID4 PPI assay. Mean BRET units normalized to NanoLuc alone in each experiment are shown for interactions between GID4 and DDX21-NL, DDX50-NL, NanoLuc. One-way analysis of variance revealed a significant interaction effect for protein and treatment on normalized BRET units ($F(2) = 19.46$, $P = 6.83 \times 10^{-6}$). Tukey's honest significant difference test for multiple comparisons was done to identify differences between DMSO and PFI-7 treated samples. Error bars indicate standard deviation. Data are from four ($n = 4$, DDX21), five ($n = 5$, DDX50) and seven ($n = 7$, NanoLuc) independent experiments. SPC, spectral counts.

bind via the GID4 substrate binding pocket by performing GID4 proximity-dependent biotinylation in the presence of proteasome inhibitor and in the presence and absence of PFI-7. Biotinylated proteins were quantified by LC–MS/MS in three groups; (1) cells expressing BioID2 treated with dimethylsulfoxide (DMSO) (vehicle), (2) cells expressing BioID2-GID4 treated with DMSO, (3) cells expressing BioID2-GID4 treated with PFI-7. Treatment with PFI-7 broadly reduced BioID2-GID4 interactions, with the number of high-confidence GID4 interactors decreasing from 77 to 13 ($\text{SP} \geq 0.9$, Fig. 4a, Supplementary Data). Samples clustered by treatment group in UMAP and principal component analyses (PCA) (Fig. 4b). PFI-7 treatment of BioID2-GID4 samples caused them to cluster closer to BioID2 alone control samples than to DMSO-treated BioID2-GID4 cells (Fig. 4b). Six GID4 interactors were maintained, and a single interactor was gained after PFI-7 treatment (Fig. 4c). We reasoned that GID4 interactors lost after PFI-7 treatment would represent candidate targets of the Pro/N-degron pathway. Overall, there were 45 high-confidence interactors in DMSO-treated BioID2-GID4 cells that were significantly depleted in PFI-7 treated samples and fell below the medium confidence threshold including DDX17, DDX21, DDX50 and KIN, among others ($\text{SP}_{\text{BioID2-GID4 DMSO}} \geq 0.9$, $\text{BioID2-GID4 PFI-7} < 0.6$, Fig. 4c). Functional annotation of GID4 interactors lost on PFI-7 treatment revealed an enrichment of gene ontology terms associated with nucleic acid binding, ribosome biogenesis and the nucleus (Fig. 4d).

To gain insights into the sequence specificity of the GID4-mediated interactions and to identify potential targets of the Pro/N-degron pathway in humans, we examined the N-terminal sequences of PFI-7-dependent GID4 interactors. The N termini of GID4 interactors DDX17, DDX21 and DDX50 matched a previously identified human GID4 Pro/N-degron sequence¹¹ (N-terminal Pro followed by one of Ser/His/Thr/Ala¹¹'Pro/N-degron', Fig. 4c). One lost interactor matched a previously described more flexible Pro/N-degron²⁶ containing a hydrophobic amino acid (P/I/L/F/V) followed by a small side-chain residue (S/T/G/V/A, 'flexible degron', Fig. 4c). Other interactors harbored Pro/N-degrons or flexible degrons within the first ten amino acids ('Pro/N-degron (if trimmed)' and 'flexible degron (if trimmed)', Fig. 4c). The consensus sequence of the N termini of high-confidence lost interactors was distinct from both the canonical Pro/N-degron¹¹, flexible degron²⁶ and other described GID4 recognition sequence²⁷ (Fig. 4e). Pro and Gly were slightly overrepresented in the N-terminal sequences of high-confidence lost interactors at position one and within the first ten amino acids, but this was not significantly different compared to the distribution of N-terminal amino acids in the proteome (Chi-squared test, d.f. = 19, $P = 0.810$, 0.378, respectively, Fig. 4f). SPC, spectral counts.

GID4 interactors DDX21 and DDX50 that were lost on PFI-7 treatment bear N termini that are evolutionarily conserved and match the canonical Pro/N-degron. DDX21 was the most highly enriched high-confidence GID4 interactor by spectral counts (BioID2-GID4 DMSO mean spectral counts 72, Supplementary Data), and both proteins interacted significantly less with GID4 after PFI-7 treatment ($\text{SP} < 0.31$, Fig. 4g). The interaction between GID4 and DDX21 and DDX50 was confirmed by (1) an orthogonal NanoBRET PPI assay in live cells using full-length C-terminally NanoLuc-tagged DDX21 or DDX50 and HaloTag-GID4 (Figs. 4h) and (2) by western blot analysis of FLAG-tagged GID4 coimmunoprecipitations (Extended Data Fig. 4a). This interaction was blocked by PFI-7 treatment (Fig. 5h and Extended Data Fig. 4a). Furthermore, DDX21 and DDX50 were found to be in a complex with endogenous RanBP9 in coimmunoprecipitation experiments dependent on ARMC8, confirming the endogenous CTLH complex interacts with DDX21 and DDX50 through GID4 (Extended Data Fig. 4b). FLAG-GID4 colocalized with DDX21/DDX50 in the nucleolus, and this colocalization was preserved after PFI-7 treatment (Extended Data Fig. 4c,d), indicating that specific GID4-DDX21–50 interactions were blocked despite their subnuclear colocalization being maintained.

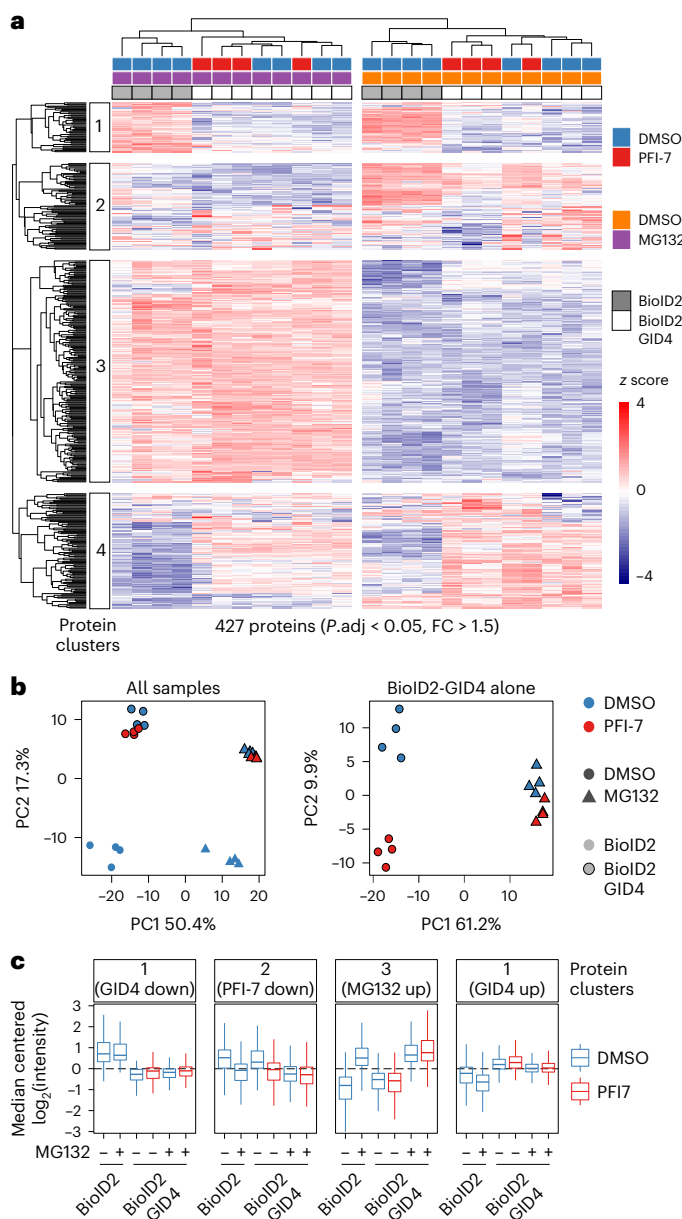


Fig. 5 | PFI-7 treatment alters the proteome of GID4-BioID2 HeLa cells.

a, Heatmap of 427 differentially abundant proteins (adjusted $P < 0.05$, fold change >1.5 , statistics derived from DEP package, Methods). Each row represents one protein and samples are represented in columns. Protein abundance is shown as z scores quantified across rows. Hierarchical clustering of samples and proteins is shown. $n = 4$ independent experiments. b, PCA of all samples (left) and BioID2-GID4 samples alone (right). DMSO-treated samples are indicated in blue and PFI-7-treated samples are shown in red. Samples treated with proteasome inhibitor (MG132) are indicated by triangles, and control samples are shown as circles. Shapes with a black outline represent BioID2-GID4 samples, while BioID2 alone samples have no outer shape color. $n = 4$ independent experiments.

c, Median protein abundance for significantly changed proteins in each cluster for each treatment group. DMSO-treated samples are shown in blue and PFI-7 treated samples are shown in red. Boxplot midline indicates median values, bounds of the box indicate 25th and 75th percentiles, and maxima and minima indicate the largest point above or below 1.5× interquartile range. Outlying points are not shown. All proteins were significantly changed (adjusted $P < 0.05$, fold change >1.5 , statistics derived from DEP package, Methods) and expression pattern trends among clusters of significantly changed proteins is indicated without secondary statistical testing. Expression is shown for 427 significantly changed proteins quantified over $n = 4$ independent experiments. Cluster sizes are as follows: cluster 1 contains 45 proteins, cluster 2 has 78 proteins, cluster 3 comprises 200 proteins and cluster 4 includes 104 proteins.

Overall, GID4 specifically binds to proteins associated with ribosomal biogenesis including Pro/N-degron-bearing nucleolar RNA helicases DDX17, DDX21 and DDX50, and PFI-7 blocks these interactions.

Regulation of protein levels by GID4

In *S. cerevisiae* GID4 is responsible for polyubiquitylating and degrading gluconeogenic enzymes Fbp1, Icl1, Mdh2 (ref. 9). However, the role GID4 plays in proteome regulation in humans is not clear. Since GID4 interacted with dozens of proteins in proximity-dependent biotinylation experiments, next we undertook a proteomics survey to determine the impact of GID4 overexpression on the proteome in the presence and absence of PFI-7 and MG132 (Extended Data Fig. 5a). Overall, 6,068 proteins were quantified across all samples (per sample mean 5,427, standard deviation 63, minimum quantified proteins 5,331, Extended Data Fig. 5b and Supplementary Data). Protein levels of CTLH complex members were stable across treatments with the exception of GID4, which was significantly higher in BioID2-GID4 cells compared to BioID2 cells (Extended Data Fig. 5c). Comparing across all treatment conditions, 427 proteins exhibited differential abundance ($FC > 1.5$, adjusted $P < 0.05$, Supplementary Data). Unsupervised hierarchical clustering of proteomics samples based on differentially abundant proteins revealed strong segregation based on proteasome inhibition and GID4 overexpression, with less robust clustering observed between PFI-7 and DMSO-treated samples (Fig. 5a). PCA revealed that proteasomal inhibition was the dominant driver of differential protein levels between groups (PC1, 50.4% of variance for all samples, 61.2% for BioID2-GID4 alone, Fig. 5b), with GID4 overexpression representing the second largest effect (PC2, 17.3% of variance for all samples). PFI-7 treatment led to distinct clustering of BioID2-GID4 samples that was reduced when proteasome function was inhibited (PC2, 9.9% of variance for BioID2-GID4, Fig. 5b). Differentially abundant proteins clustered broadly into four groups (Fig. 5a). Proteins that increased on proteasomal inhibition were located in cluster 3. GID4 overexpression decreased average levels of proteins within cluster 1, while increasing levels of proteins in cluster 4 (Fig. 5a,c). Cluster 2 contained proteins that decreased on average after PFI-7 treatment of BioID-GID4 cells, and this change was blocked by proteasomal inhibition (Fig. 5a,c). PFI-7 treatment led to a greater number of significantly changed proteins in cells with proteasomal function intact (60 differential proteins, $FC > 1.5$, adjusted $P < 0.05$) compared to cells treated with proteasome inhibitor (15 differential proteins). Thus, PFI-7 likely modulates protein homeostasis via a proteosome-dependent mechanism.

PFI-7 treatment significantly increased levels of DHX40 and DICER1, while decreasing others including KIN and CHAF1A (Fig. 6a,b). GID4 overexpression altered levels of DDX39A and nucleolar protein

IFI16 that were both increased, and EIF4A2 and LMNB2 that both decreased Fig. 6a,b). There were similar numbers of protein-level changes after GID4 overexpression with proteasomal function intact (55 proteins $FC > 1.5$, adjusted $P < 0.05$) or inhibited (62 proteins $FC > 1.5$, adjusted $P < 0.05$) (Fig. 6a). DDX21 and DDX50 protein levels were consistent irrespective of GID4 overexpression or PFI-7 treatment (Fig. 6a,b). PFI-7-dependent proteins included four that were identified as medium confidence GID4 interactors (BioID2-GID4 SP ≥ 0.6) including KIN, WEE1, HMGCS1 and CHAF1A, and two that contained Pro/N-degrons, HMGCS1 and ASA1 (Fig. 6b and Extended Data Fig. 5d). Eight proteins altered after GID4 overexpression were identified as GID4 interactors including DDX39A and IFI16, and three contained Pro/N-degrons (Fig. 6b and Extended Data Fig. 5d).

As HMGCS1 was increased by PFI-7 treatment, has a conserved Pro/N-degron, and was a medium confidence GID4 interactor (Fig. 6c and Extended Data Fig. 5d), it emerged as a candidate degradation target of the human Pro/N-degron pathway. Indeed, we confirmed by western blot that treatment with PFI-7, but not PFI-7N, resulted in increased levels of HMGCS1 (Fig. 6d). Additionally, cycloheximide chase experiments revealed that PFI-7 treatment significantly attenuated HMGCS1 protein turnover compared to treatment with PFI-7N (Fig. 6e). Taken together, despite disrupting their interactions with GID4, protein levels of DDX21 and DDX50 levels remain similar after GID4 inhibition with PFI-7 while significant changes are observed in levels of other proteins including HMGCS1, DHX40 and DICER1.

Discussion

PFI-7 is a chemical probe targeting GID4, the substrate receptor of the CTLH ubiquitin ligase complex. As a high-quality chemical probe^{34–37} PFI-7 is potent (K_d of 79 ± 7 nM by SPR) and active in cells at $1 \mu\text{M}$ (Nano-BRET GID4 MPGLWKS-NL PPI IC₅₀ = $0.57 \pm 0.05 \mu\text{M}$). PFI-7 showed no evident cytotoxicity and no significant off-target activity by chemoproteomics and against a panel of proteins such as kinases, GPCRs and other drug safety targets. The cellular activity and specific target engagement by PFI-7 is evident from the robust changes observed in GID4 interactions and proteome level regulation. Since the E3 ligase activity of the human CTLH complex has only recently been demonstrated^{20,22}, and it is unclear what role GID4-mediated substrate recruitment and proteasomal degradation plays in the array of fundamental cellular processes in which the complex has been implicated¹⁴, we analyzed global proteomics and the interactome of GID4 in the presence and absence of PFI-7 to probe the function of GID4 and the CTLH complex. We demonstrate candidate degradation targets of GID4 such as HMGCS1 while other proteins such as RNA helicases DDX21 and DDX50 are recognized by GID4 but are not substantively regulated at the protein level. This

Fig. 6 | GID4- and PFI-7-dependent changes in RNA helicases and HMGCS1.

a, Volcano plot of all proteins with \log_2 fold change shown on the x axis and $-\log_{10}$ adjusted P values shown on the y axis. The number of significantly changed proteins is indicated in the top corner. Specific proteins of interest are labeled and indicated by red dots. Adjusted P values were derived from DEP package (Methods) and were adjusted using Benjamini–Hochberg procedure. $n = 4$ independent experiments. **b**, Median-centered \log_2 intensities for specific proteins that were changed by PFI-7, GID4 or unchanged by either. First ten amino acids of N termini are indicated below protein names. Gray boxplot outlines represent BioID2 alone samples, black boxplot outlines represent BioID2-GID4 samples. Blue dots represent DMSO-treated samples and red dots indicate PFI-7 treated samples. Circles plotted above each protein name represents enrichment in the BioID2-GID4 experiment indicated in Fig. 5. Proteins with no circles above were not quantified in BioID2-GID4. Boxplot midline indicates median values, bounds of the box indicate 25th and 75th percentiles, and maxima and minima indicate the largest point above or below the $1.5 \times$ interquartile range. $n = 4$ independent experiments. **c**, Top, multi-species alignment showing conservation of Pro/N-degron sequence at the N terminus of HMGCS1. Below, median-centered \log_2 intensities of HMGCS1 in whole proteome data from BioID2-GID4 samples

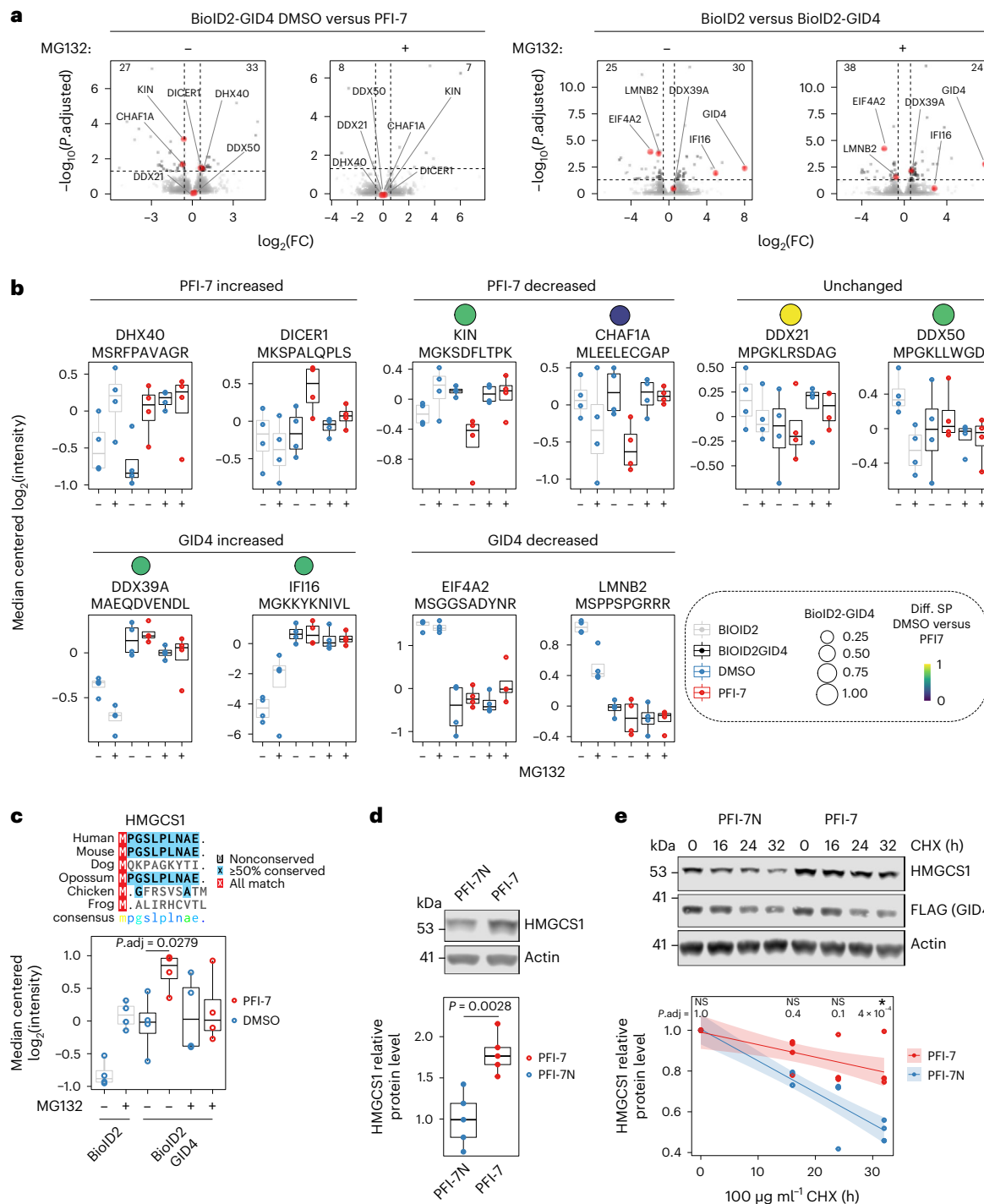
treated with PFI-7 or DMSO control in the presence or absence of proteasome inhibitor. Adjusted P values were derived from the DEP package (Methods) and were adjusted using the Benjamini–Hochberg procedure. $n = 4$ independent experiments. **d**, Western blot quantification of HMGCS1 protein levels in HEK293T cells. A representative western blot is shown (top) with quantification from $n = 5$ independent experiments indicated below. A significant P value ($P = 0.0028$) was derived from Welch's unpaired two-tailed t -test. **e**, Western blot quantification of HMGCS1 protein levels in a cycloheximide (CHX) pulse-chase in HEK293T cells inducibly overexpressing FLAG-GID4. A representative western blot is shown (top) and quantification is shown from $n = 5$ independent experiments below. A two-way analysis of variance revealed a significant interaction between $50 \mu\text{g } \mu\text{l}^{-1}$ CHX treatment time and PFI-7/PFI-7N treatment ($F(3, 24) = 4.80, P = 0.0093$). Post hoc comparisons using Tukey's honestly significant difference test indicated that PFI-7 treatment significantly increased HMGCS1 protein level at 32 h CHX compared to PFI-7N (adjusted $P = 4 \times 10^{-4}$). Linear models were fit to the data using least squares method with each solid line indicating the best fit to the data and 95% confidence intervals indicated by the surrounding shaded area. Diff, differential; NS, not significant.

suggests that CTLH-GID4 may have degradative and nondegradative functions highlighting potential challenges for using the CTLH complex for targeted protein degradation^{8,29}. Thus, the unique advantages afforded through use of a potent and selective chemical probe provides new insights into GID4 and the CTLH complex.

Our proximity-dependent biotinylation analysis defined the GID4 interactome, complementing the rapidly growing numbers of interactomes for human proteins^{33,38,39}. We demonstrate a strong tendency for GID4 to interact with nuclear and nucleolar proteins, which is supported by the immunofluorescence subcellular localization of exogenously expressed GID4. As the CTLH complex has been reported to form nuclear-specific complexes⁴⁰, GID4 may be recruiting the CTLH complex to targets in the nucleus and nucleolus. One caveat of traditional

proximity-dependent biotinylation studies is that both direct and indirect interactors will be biotinylated^{41,42}. PFI-7, however, facilitated the identification of proteins, or their interactors, that bind directly via the GID4 substrate binding pocket. Interactors that were lost on PFI-7 treatment included RNA helicases DDX17, DDX21 and DDX50 that have previously been reported to associate with the CTLH complex^{18,20,38,40}, and that we now show are GID4-dependent interactors. Indeed, many of the direct GID4 interactors are nucleolar proteins including DDX21 (ref. 43), DDX50 (ref. 44) and KIN⁴⁵, among others. This points to possible nucleolar-specific functions of the CTLH complex that have been suggested previously⁴⁰ and remain to be elucidated further.

Several of the nucleolar RNA helicases that interact with GID4 bear consensus Pro/N-degron sequences that agree with previously



identified GID4 recognition sequences¹¹ including DDX17, DDX21 and DDX50. Many other interactors did not contain the canonical Pro/N-degron. There are several plausible explanations for this. First, it has been suggested that the sequences GID4 binds to may be flexible and tolerate non-Pro hydrophobic residues^{26,27}. In addition, specific N-terminal aminopeptidases were recently shown to trim protein N termini to allow recognition of internal Pro/N-degrons in *S. cerevisiae*⁴⁶. The aminopeptidases identified are conserved in humans⁴⁶ suggesting that some of the GID4 interactors identified that lack N-terminal recognition sequences might have been processed by aminopeptidases to reveal internal sequences that are recognized by GID4. Also, interactors might engage GID4 indirectly via intermediary proteins that carry conventional GID4 recognition sequences. The GID4 interactors we describe will inform future work to explain the seemingly diverse GID4-mediated recruitment mechanisms of the CTLH complex.

In addition to providing new insights into GID4 interactors, using PFI-7 we also characterized proteome level regulation by GID4. This analysis revealed HMGCS1 as a canonical Pro/N-degron protein affected by PFI-7. HMGCS1 is a rate-limiting enzyme in the mevalonate pathway that metabolizes acetyl-CoA into sterols and isoprenoids essential for cancer cell survival and growth⁴⁷. HMGCS1 as a target of GID4 aligns with the metabolic functions of the Gid/CTLH complex reported in various species^{12,14,25}. In addition, we show that GID4 plays a role in regulating the cellular abundance of dozens of proteins including RNA helicase DHX40 and ribonuclease DICER1. Since GID4 antagonism with PFI-7 increased the levels of these proteins and this effect was blocked by proteasomal inhibition, this argues that GID4 is required for proteasomal degradation of DHX40 and DICER1. However, neither protein appears to interact with GID4 in our proximity-dependent biotinylation experiments, suggesting that they do not directly interact with GID4, that their interaction topology is inconsistent with biotinylation or that substrate lysines are not available to be biotinylated. Since we found that GID4 binds to several RNA helicases, a protein family known to facilitate multivalent interactions⁴⁸, it is plausible that DHX40 and DICER1 might be binding to GID4 in complexes containing multiple RNA helicases. In support of this, DICER1 is a ribonuclease of the helicase family that interacts with an array of RNA binding proteins including RNA helicase DDX17 (refs. 49,50). DDX17 is a GID4 interactor lost on PFI-7 treatment, bears a canonical N-terminal GID4 recognition sequence (PTGFVAPIL) and has previously been shown to interact with CTLH RING-domain subunit MAEA³⁸. Similarly, DHX40 is a member of the DEAH-box family of RNA helicases⁵¹ that has previously been identified as an interactor of DDX23 (ref. 33) and DDX24 (ref. 52), both of which we identified as GID4 interactors (SP DDX23, 0.67; SP DDX24, 1.0). Together, this suggests that protein-level regulation of specific targets might occur via indirect interactions mediated by intermediary proteins such as RNA helicases.

While the abundances of dozens of proteins were altered by PFI-7 treatment, most GID4 interactors were not affected. Protein-level regulation of DDX21 and DDX50 was absent, for instance, suggesting that their interaction with GID4 might impart other functions rather than polyubiquitylation-mediated degradation. In addition to proteasomal degradation, ubiquitylation is also associated with altered protein interactions and localization, among other functions⁵³. In agreement with our identification of nondegradative GID4 interactions, ubiquitylation of the glycolysis enzymes PKM2 and LDHA was recently shown to be dependent on the CTLH complex, but the proteins were not degraded²⁵. The ubiquitin linkages conjugated by E3 ubiquitin ligases depend on their cognate E2 enzymes⁵³. The only E2 enzyme implicated so far in substrate ubiquitylation by the CTLH complex is UBE2H (ref. 20). We observed significant interactions between GID4 and the unique E2/E3 hybrid enzyme, UBE2O. UBE2O is associated with monoubiquitylation of an array of substrates including ribosomal proteins⁵⁴ and chromatin associated proteins⁵⁵, and has previously been shown to cofractionate with CTLH complex member WDR26 (refs. 28,56). This suggests that GID4 interactors such as DDX21/50

may be monoubiquitylated by CTLH/UBE2O to modulate their activity instead of being polyubiquitylated as a degradation signal¹⁶. Together, these data and our new results using PFI-7 indicate both regulatory and degradative roles for CTLH with its substrates, possibly depending on subcellular localization and possibly E2 partner interactions.

PFI-7 facilitated the identification of dozens of GID4 interacting proteins, several of which are not substantively regulated at the protein level while other proteins were dependent on GID4 for protein-level regulation, possibly mediated through indirect interactions with the CTLH complex. It is clear that there is much still to learn about the fundamental biology of the mammalian CTLH complex. Going forward, PFI-7 will be a valuable research tool to study the CTLH complex and its substrate receptor GID4. Our findings inform future efforts to use GID4 and the CTLH complex as an E3 ligase in targeted protein degradation.

Online content

Any methods, additional references, Nature Portfolio reporting summaries, source data, extended data, supplementary information, acknowledgements, peer review information; details of author contributions and competing interests; and statements of data and code availability are available at <https://doi.org/10.1038/s41589-024-01618-0>.

References

- Varshavsky, A. The ubiquitin system, autophagy, and regulated protein degradation. *Annu. Rev. Biochem.* **86**, 123–128 (2017).
- Varshavsky, A. N-degron and C-degron pathways of protein degradation. *Proc. Natl Acad. Sci. USA* **116**, 358–366 (2019).
- Sherpa, D., Chrustowicz, J. & Schulman, B. A. How the ends signal the end: regulation by E3 ubiquitin ligases recognizing protein termini. *Mol. Cell* **82**, 1424–1438 (2022).
- Mészáros, B., Kumar, M., Gibson, T. J., Uyar, B. & Dosztányi, Z. Degrons in cancer. *Sci. Signal* **10**, eaak9982 (2017).
- Rechsteiner, M. & Rogers, S. W. PEST sequences and regulation by proteolysis. *Trends Biochem. Sci.* **21**, 267–271 (1996).
- Collins, G. A. & Goldberg, A. L. The logic of the 26S proteasome. *Cell* **169**, 792–806 (2017).
- Gonda, D. K. et al. Universality and structure of the N-end rule. *J. Biol. Chem.* **264**, 16700–16712 (1989).
- Schapira, M., Calabrese, M. F., Bullock, A. N. & Crews, C. M. Targeted protein degradation: expanding the toolbox. *Nat. Rev. Drug Discov.* **18**, 949–963 (2019).
- Chen, S.-J., Wu, X., Wadas, B., Oh, J.-H. & Varshavsky, A. An N-end rule pathway that recognizes proline and destroys gluconeogenic enzymes. *Science* **355**, eaal3655 (2017).
- Hämmerle, M. et al. Proteins of newly isolated mutants and the amino-terminal proline are essential for ubiquitin-proteasome-catalyzed catabolite degradation of fructose-1,6-bisphosphatase of *Saccharomyces cerevisiae*. *J. Biol. Chem.* **273**, 25000–25005 (1998).
- Dong, C. et al. Molecular basis of GID4-mediated recognition of degrons for the Pro/N-end rule pathway article. *Nat. Chem. Biol.* **14**, 466–473 (2018).
- Santt, O. et al. The yeast GID complex, a novel ubiquitin ligase (E3) involved in the regulation of carbohydrate metabolism. *Mol. Biol. Cell* **19**, 3323–3333 (2008).
- Francis, O., Han, F. & Adams, J. C. Molecular phylogeny of a RING E3 ubiquitin ligase, conserved in eukaryotic cells and dominated by homologous components, the muskelin/RanBPM/CTLH complex. *PLoS ONE* **8**, e75217 (2013).
- Maitland, M. E. R., Lajoie, G. A., Shaw, G. S. & Schild-Poulter, C. Structural and functional insights into GID/CTLH E3 ligase complexes. *Int. J. Mol. Sci.* **23**, 5863 (2022).
- Melnikov, A., Chen, S.-J. & Varshavsky, A. Gid10 as an alternative N-recognin of the Pro/N-degron pathway. *Proc. Natl Acad. Sci. USA* **116**, 15914–15923 (2019).

16. Qiao, S. et al. Interconversion between anticipatory and active GID E3 ubiquitin ligase conformations via metabolically driven substrate receptor assembly. *Mol. Cell* **77**, 150–163.e9 (2020).
17. Kong, K.-Y. E. et al. Timer-based proteomic profiling of the ubiquitin-proteasome system reveals a substrate receptor of the GID ubiquitin ligase. *Mol. Cell* **81**, 2460–2476.e11 (2021).
18. Mohamed, W. I. et al. The human GID complex engages two independent modules for substrate recruitment. *EMBO Rep.* **22**, e52981 (2021).
19. Huffman, N., Palmieri, D. & Coppola, V. The CTLH complex in cancer cell plasticity. *J. Oncol.* **2019**, 4216750 (2019).
20. Lampert, F. et al. The multi-subunit GID/CTLH E3 ubiquitin ligase promotes cell proliferation and targets the transcription factor Hbp1 for degradation. *eLife* **7**, e35528 (2018).
21. Leal-Esteban, L. C., Rothé, B., Fortier, S., Isenschmid, M. & Constam, D. B. Role of bicaudal C1 in renal gluconeogenesis and its novel interaction with the CTLH complex. *PLoS Genet.* **14**, e1007487 (2018).
22. Maitland, M. E. R. et al. The mammalian CTLH complex is an E3 ubiquitin ligase that targets its subunit muskelin for degradation. *Sci. Rep.* **9**, 9864 (2019).
23. Zhen, R. et al. Wdr26 regulates nuclear condensation in developing erythroblasts. *Blood* **135**, 208–219 (2020).
24. McTavish, C. et al. Regulation of c-Raf stability through the CTLH Complex. *Int. J. Mol. Sci.* **20**, 934 (2019).
25. Maitland, M. E. R., Kuljanin, M., Wang, X., Lajoie, G. A. & Schild-Poulter, C. Proteomic analysis of ubiquitination substrates reveals a CTLH E3 ligase complex-dependent regulation of glycolysis. *FASEB J.* **35**, e21825 (2021).
26. Dong, C. et al. Recognition of nonproline N-terminal residues by the Pro/N-degron pathway. *Proc. Natl Acad. Sci. USA* **117**, 14158–14167 (2020).
27. Chrustowicz, J. et al. Multifaceted N-degron recognition and ubiquitylation by GID/CTLH E3 ligases. *J. Mol. Biol.* **434**, 167347 (2022).
28. Oughtred, R. et al. The BioGRID database: a comprehensive biomedical resource of curated protein, genetic, and chemical interactions. *Protein Sci.* **30**, 187–200 (2021).
29. Chana, C. K. et al. Discovery and structural characterization of small molecule binders of the human CTLH E3 ligase subunit GID4. *J. Med. Chem.* **65**, 12725–12746 (2022).
30. Yazdi, A. K. et al. Chemical tools for the Gid4 subunit of the human E3 ligase C-terminal to LisH (CTLH) degradation complex. *RSC Med. Chem.* **15**, 1066–1071 (2024).
31. Sherpa, D. et al. GID E3 ligase supramolecular chelate assembly configures multipronged ubiquitin targeting of an oligomeric metabolic enzyme. *Mol. Cell* **81**, 2445–2459.e13 (2021).
32. Coyaud, E. et al. BiLoD-based identification of Skp cullin F-box (SCF) β -TrCP1/2 E3 ligase substrates. *Mol. Cell Proteomics* **14**, 1781–1795 (2015).
33. Go, C. D. et al. A proximity-dependent biotinylation map of a human cell. *Nature* **595**, 120–124 (2021).
34. Arrowsmith, C. H. et al. The promise and peril of chemical probes. *Nat. Chem. Biol.* **11**, 536–541 (2015).
35. Frye, S. V. The art of the chemical probe. *Nat. Chem. Biol.* **6**, 159–161 (2010).
36. Blagg, J. & Workman, P. Choose and use your chemical probe wisely to explore cancer biology. *Cancer Cell* **32**, 268–270 (2017).
37. Vu, V., Szewczyk, M. M., Nie, D. Y., Arrowsmith, C. H. & Barsyte-Lovejoy, D. Validating small molecule chemical probes for biological discovery. *Annu. Rev. Biochem.* **91**, 61–87 (2022).
38. Huttlin, E. L. et al. Dual proteome-scale networks reveal cell-specific remodeling of the human interactome. *Cell* **184**, 3022–3040.e28 (2021).
39. Cho, N. H. et al. OpenCell: endogenous tagging for the cartography of human cellular organization. *Science* **375**, eabi6983 (2022).
40. Onea, G., Maitland, M. E. R., Wang, X., Lajoie, G. A. & Schild-Poulter, C. Distinct nuclear and cytoplasmic assemblies and interactomes of the mammalian CTLH E3 ligase complex. *J. Cell Sci.* **135**, jcs259638 (2022).
41. Kim, D. I. et al. Probing nuclear pore complex architecture with proximity-dependent biotinylation. *Proc. Natl Acad. Sci. USA* **111**, E2453–E2461 (2014).
42. Gingras, A.-C., Abe, K. T. & Raught, B. Getting to know the neighborhood: using proximity-dependent biotinylation to characterize protein complexes and map organelles. *Curr. Opin. Chem. Biol.* **48**, 44–54 (2019).
43. Calo, E. et al. RNA helicase DDX21 coordinates transcription and ribosomal RNA processing. *Nature* **518**, 249–253 (2015).
44. Zhang, Y., Forys, J. T., Miceli, A. P., Gwinn, A. S. & Weber, J. D. Identification of DHX33 as a mediator of rRNA synthesis and cell growth. *Mol. Cell. Biol.* **31**, 4676–4691 (2011).
45. Gaspar, V. P. et al. Interactome analysis of KIN (Kin17) shows new functions of this protein. *Curr. Issues Mol. Biol.* **43**, 767–781 (2021).
46. Chen, S.-J., Kim, L., Song, H. K. & Varshavsky, A. Aminopeptidases trim Xaa-Pro proteins, initiating their degradation by the Pro/N-degron pathway. *Proc. Natl Acad. Sci. USA* **118**, e2115430118 (2021).
47. Mullen, P. J., Yu, R., Longo, J., Archer, M. C. & Penn, L. Z. The interplay between cell signalling and the mevalonate pathway in cancer. *Nat. Rev. Cancer* **16**, 718–731 (2016).
48. Hondele, M. et al. DEAD-box ATPases are global regulators of phase-separated organelles. *Nature* **573**, 144–148 (2019).
49. Hansen, S. R., Aderounmu, A. M., Donelick, H. M. & Bass, B. L. Dicer's helicase domain: a meeting place for regulatory proteins. *Cold Spring Harb. Symp. Quant. Biol.* **84**, 185–193 (2019).
50. Gregory, R. I. et al. The Microprocessor complex mediates the genesis of microRNAs. *Nature* **432**, 235–240 (2004).
51. Abdelhaleem, M., Maltais, L. & Wain, H. The human DDX and DHX gene families of putative RNA helicases. *Genomics* **81**, 618–622 (2003).
52. Georges, A., Marcon, E., Greenblatt, J. & Frappier, L. Identification and characterization of USP7 targets in cancer cells. *Sci. Rep.* **8**, 15833 (2018).
53. Komander, D. & Rape, M. The ubiquitin code. *Annu. Rev. Biochem.* **81**, 203–229 (2012).
54. Nguyen, A. T. et al. UBE2O remodels the proteome during terminal erythroid differentiation. *Science* **357**, eaan0218 (2017).
55. Mashitalir, N. et al. Autodeubiquitination protects the tumor suppressor BAP1 from cytoplasmic sequestration mediated by the atypical ubiquitin ligase UBE2O. *Mol. Cell* **54**, 392–406 (2014).
56. Havugimana, P. C. et al. A census of human soluble protein complexes. *Cell* **150**, 1068–1081 (2012).

Publisher's note Springer Nature remains neutral with regard to jurisdictional claims in published maps and institutional affiliations.

Springer Nature or its licensor (e.g. a society or other partner) holds exclusive rights to this article under a publishing agreement with the author(s) or other rightsholder(s); author self-archiving of the accepted manuscript version of this article is solely governed by the terms of such publishing agreement and applicable law.

© The Author(s), under exclusive licence to Springer Nature America, Inc. 2024

¹Structural Genomics Consortium, University of Toronto, Toronto, Ontario, Canada. ²Robarts Research Institute, Schulich School of Medicine and Dentistry, University of Western Ontario, London, Ontario, Canada. ³Department of Biochemistry, Schulich School of Medicine and Dentistry, University of Western Ontario, London, Ontario, Canada. ⁴Don Rix Protein Identification Facility, Schulich School of Medicine and Dentistry, University of Western Ontario, London, Ontario, Canada. ⁵Institute of Molecular Systems Biology at ETH Zurich, Zurich, Switzerland. ⁶Institut für Pharmazeutische Chemie, Goethe-University Frankfurt, Biozentrum, Frankfurt am Main, Germany. ⁷Structural Genomics Consortium, Goethe-University Frankfurt, Buchmann Institute for Life Sciences, Frankfurt am Main, Germany. ⁸Development and Medical, Pfizer Worldwide Research, Groton, CT, USA. ⁹Department of Pharmacology and Toxicology, University of Toronto, Toronto, Ontario, Canada. ¹⁰Department of Physiology, University of Toronto, Toronto, Ontario, Canada. ¹¹Hubei Key Laboratory of Genetic Regulation and Integrative Biology, School of Life Sciences, Central China Normal University, Wuhan, China. ¹²Department of Medical Biophysics, University of Toronto, Toronto, Ontario, Canada. ¹³Princess Margaret Cancer Centre, University Health Network, Toronto, Ontario, Canada. ¹⁴These authors contributed equally: Dominic D. G. Owens, Matthew E. R. Maitland.  e-mail: Cheryl.Arrowsmith@uhn.ca

Methods

Expression, purification and structure determination of GID4

The GID4 protein was expressed, purified and crystallized exactly as reported previously¹¹. X-ray diffraction data for GID4 + UBPF023596 (alternate name of PFI-7 at the time of Protein Data Bank (PDB) deposition) were collected at 100 K at beamline 24ID-C of Advanced Photon Source, Argonne National Laboratory. The data were processed using XDS⁵⁷ and the HKL-3000 suite⁵⁸ respectively, and the structure was solved by molecular methods using PDB 6WZZ as a search template with the program PHASER⁵⁹. REFMAC⁶⁰ and BUSTER⁶¹ were used for structure refinement. Geometry restraints for the compound refinement were prepared with by GRADE developed at Global Phasing Ltd⁶². Graphics program COOT⁶³ was used for model building and visualization. Molprobity⁶⁴ was used for structure validation. For *in vivo* biotinylation of GID4 used for biophysical assays, DNA fragment encoding Biotinylated-GID4 (amino acids (aa) 116–300) was amplified by PCR and subcloned into pET 28BIOH-LIC vector, downstream of the AviTag and a C-terminal 6× HIS tag⁶⁵. The protein was overexpressed in *Escherichia coli* BL21 (DE3) containing BirA using biotin-supplemented Terrific Broth media. Cells were lysed and protein was purified using Nickel affinity chromatography, and during the purification an extra wash step was done with washing buffer that included 1 mM D-biotin, followed by size-exclusion chromatography using a HiLoadTM 26/60 Superdex 75 gel filtration column (GE Healthcare).

Analysis of binding by SPR

In vitro binding analyses by SPR were carried out using a Biacore T200 (GE Health Sciences Inc.) instrument at 25 °C. HBS-EP+ buffer (10 mM HEPES pH 7.4, 150 mM NaCl, 3 mM EDTA, 0.05% Tween-20) was used for all the experiments. The N-terminally *in vivo* Biotinylated-GID4 (aa 116–300) was immobilized to approximately 2,100 response units (RU) on a flow cell of a Streptavidin-coated sensor chip (GE healthcare) according to the manufacturer's directions while another flow cell was left blank for reference subtraction and monitoring any nonspecific bindings. The compounds were diluted in HBS-EP+ to yield a 1% final DMSO solution and were serially diluted (threefold dilutions) in HBS-EP+ buffer containing 1% DMSO. The compounds were then flowed over the sensor chip using a MultiCycle Kinetics mode at 40 µl min⁻¹. Contact time (that is, association phase) was 60 s and disassociation time was 120 s, which was followed by an additional 120 s of stabilization period under flow. HBS-EP+ buffer only (plus 1% DMSO) was used for blank injections, and HBS-EP+ buffers containing 0.5 to 1.5% DMSO were used for solvent correction injections. Binding constants were acquired from the double referenced (that is, reference subtraction and blank injection subtraction) multicycle data using Biacore T200 Evaluation Software v.3.1.

Fluorescence polarization-based peptide displacement assay

The fluorescence polarization-based peptide displacement experiments were performed in 384-well polypropylene small volume black microplates (cat. no. 784209, Greiner) in a total volume of 15 µl per well at room temperature (that is, 23 °C). Compounds were added to the reaction mixture (containing 5 µM GID4 (aa 116–300) and 40 nM of C-terminally fluorescein isothiocyanate-labeled PGLWKS peptide in buffer (50 mM Tris, pH 7.5 and 0.01% Triton X-100)), and were incubated for 30 min at room temperature. Final DMSO concentration was 1.5%. The resulting fluorescence polarization signals were measured using a BioTek Synergy 4 (BioTek) at the excitation and emission wavelengths of 485 and 528 nm, respectively. The obtained fluorescence polarization values were blank subtracted and are shown as the percentage of control. All the experiments were carried out in triplicate ($n = 3$) and the presented values are the average of replicates ± standard deviation. Fluorescence polarization data were visualized using GraphPad Prism software v.8.0.

Cell culture

Cell lines were cultured according to standard aseptic mammalian tissue culture protocols in 5% CO₂ at 37 °C. HEK293 and HeLa cells were cultured in DMEM supplemented with 10% fetal bovine serum (FBS) and 100 U ml⁻¹ penicillin and 100 µg ml⁻¹ streptomycin. HeLa cells transiently transfected with the BioID2 plasmid constructs or HA-GID4 was done using jetPRIME transfection reagent (Polyplus-transfection), following the manufacturer's instructions and either collected after 24 h for immunoblotting or fixed and permeabilized for immunofluorescence. For generation of T-REx-HeLa inducible BioID2 cell lines, 1.5 µg of DNA (1,350 ng of pOG44 plasmid and 150 ng of pCDNA5/FRT/TO/HA-myc-BIOID2-GID4 or pCDNA5/FRT/TO/HA-myc-BIOID2) was used to transfect one well of a six-well plate of Flp-In T-Rex HeLa doxycycline-inducible cells (generated by A. Desai's laboratory, San Diego, CA, USA). On day 3, cells were selected with 200 µg ml⁻¹ hygromycin and 3 µg ml⁻¹ blasticidin until day 17 when colonies were collected. Expression was induced with 1 µg ml⁻¹ doxycycline. For generation of HEK293T cells expressing FLAG-tagged GID4, lentiviral particles were generated by transfecting 5 × 10⁵ cells, which had been seeded into a six-well plate 24 h before. For transfection, 0.6 µg of PAX2 and 0.3 µg of VSVG vector were used with the XtremeGeneHP reagent (Sigma, cat. no. 6366236001), according to the manufacturer's protocol. Then 24 h posttransfection, the media was replaced. The media was then collected at 48 and 72 h, filtered through a 0.45 µm filter, and centrifuged to remove cells. A 500 µl aliquot of the filtered supernatant, which contained the viral particles, was used to infect a fresh well of 5 × 10⁵ parental HEK293T cells. Media of the infected cells was changed after 24 h. Following another 24 h period, puromycin selection was conducted for 72 h at a concentration of 1.5 µg ml⁻¹.

Cell extracts

For HMGCS1 immunoblots, cells were lysed in lysis buffer (20 mM Tris-HCl pH 8, 150 mM NaCl, 1 mM EDTA, 10 mM MgCl₂, 0.5% Triton X-100, 12.5 U ml⁻¹ benzonase). After 2 min of incubation at room temperature, SDS was added to final 1% concentration. For nuclear and cytoplasmic fractionation of lysates, cells were lysed in cytoplasmic lysis buffer (50 mM HEPES pH 7.4, 150 mM NaCl) supplemented with 10 µg ml⁻¹ aprotinin (BioShop), 2 µg ml⁻¹ leupeptin (BioShop), 2.5 µg ml⁻¹ pepstatin (BioShop), 1 mM dithiothreitol (DTT), 2 mM NaF, 2 mM Na₃VO₄, 0.1 mM phenylmethylsulfonyl fluoride (PMSF) and 75 µg ml⁻¹ digitonin (Sigma-Aldrich). After 10 min of incubation on ice, samples were centrifuged at 2,000g for 1 min and the resulting supernatant was saved as the cytoplasmic lysate. The resulting pellet was resuspended with nuclear lysis buffer (10 mM Tris-HCl pH 8.0, 100 mM NaCl, 0.1% sodium deoxycholate, 1 mM EDTA, 25% glycerol) supplemented with 10 µg ml⁻¹ aprotinin, 2 µg ml⁻¹ leupeptin, 2.5 µg ml⁻¹ pepstatin, 1 mM DTT, 2 mM NaF, 2 mM Na₃VO₄, 0.1 mM PMSF and 100 U ml⁻¹ benzonase nuclease (E1014-5KU, Sigma-Aldrich) and incubated on ice for 30 min. Samples were then centrifuged at 17,000g for 20 min to collect the nuclear fraction. For all other immunoblots, cells were lysed in whole-cell extract buffer (50 mM NaCl, 50 mM HEPES (pH 7.4), 1 mM EDTA, 10% glycerol, 0.5% Nonidet P-40) supplemented with the same inhibitors as above.

Plasmids

To generate BioID2-GID4, GID4 complementary DNA was digested from the pEZ-M06 GID4 plasmid²² using Pmel and EcoRI restriction enzymes and ligated into HpaI and EcoRI-digested MYC-BioID2-MCS (Addgene plasmid, cat. no. 74223). An HA tag was subcloned 5' to the MYC tag in the BioID2-GID4 plasmid as well as for negative control BioID2 alone vector. For generation of T-REx-293 inducible BioID2 cell lines, The HA-myc-BioID2-GID4 construct was cloned into pCDNA5/FRT/TO vector. N-terminally FLAG-tagged GID4 (FLAG-GID4) was cloned into a modified pSTV6 lentiviral vector. For insertion of FLAG-GID4 into the multiple cloning site of pSTV6, restriction cloning was performed using AgeI and XbaI enzymes. For NanoBRET PPI assays, GID4

coding sequence was cloned in frame into pNLF1-N for GID4-NanoLuc N-terminal fusion, into pNLF1-C for GID4-NanoLuc C-terminal fusion, or into pHNT-HaloTag vector for GID4-HaloTag N-terminal fusion using the In-Fusion HD Cloning kit (Takara). The Pro/N-degron coding sequence was cloned into pNLF1-C for MPGLWKS-NanoLuc C-terminal fusion. All backbone vectors were obtained from Promega before cloning and sequence verified to confirm desired cloned constructs.

NanoBRET

NanoBRET live cell target engagement. The assay was performed essentially as described in ref. 66. Full-length GID4 N- or C-terminal NanoLuc fusion was transfected into HEK293T cells using FuGENE HD (Promega, cat. no. E2312) according to the manufacturer's instructions and proteins were allowed to express for 20 h. Serially diluted PFI-7 and GID4-tracer at a concentration of 1 μ M were pipetted into white 384-well plates (Greiner 781207) using an Echo acoustic dispenser (Labcyte). The corresponding protein-transfected cells were added and reseeded at a density of 2×10^5 cells per ml after trypsinization and resuspending in Opti-MEM without phenol red (Life Technologies). The system was allowed to equilibrate for 2 h at 37 °C/5% CO₂ before BRET measurements. To measure BRET, NanoBRET NanoGlo Substrate + Extracellular NanoLuc Inhibitor (Promega, cat. no. N2540) was added as per the manufacturer's protocol. Filtered luminescence was measured on a PHERAstar plate reader (BMG Labtech) equipped with a luminescence filter pair (450 nm band-pass filter (donor) and 610 nm long-pass filter (acceptor)). Competitive displacement data were graphed using GraphPad Prism v.9 software using a normalized three-parameter curve fit with the following equation: $y = 100/(1 + 10^{(x - \log IC_{50})})$.

NanoBRET PPI assay. For NanoBRET PPI assays, HEK293T cells plated in 96-well white plastic plates (Greiner) were transfected with 10 ng NanoLuc protein (N-terminally tagged with MPGLWKS, full-length DDX21 or full-length DDX50) and 50 ng of N-terminally tagged HaloTag-GID4 using X-tremeGENE HP DNA Transfection Reagent (Sigma), following the manufacturer's instructions. The next day, the media was replaced with DMEM/F12 (no phenol red) supplemented with 4% FBS, penicillin (100 U ml⁻¹) and streptomycin (100 μ g ml⁻¹) in the presence or absence of compounds and HaloTag NanoBRET 618 Ligand (Promega) for 4 h. Next, NanoBRET NanoGlo Substrate (Promega) solution was added to each well. Donor emission at 450 nm (filter, 450 nm/band-pass 80 nm) and acceptor emission at 618 nm (filter, 610 nm per long-pass) was measured within 10 min of substrate addition using a CLARIOstar microplate reader (Mandel). mBU values were calculated by subtracting the mean of 618/460 signal from cells without a NanoBRET 618 Ligand \times 1,000 from the mean of 618/460 signal from cells with a NanoBRET 618 Ligand \times 1,000.

Chemoproteomics

HeLa cells expressing GID4-BioID2 were induced with 1.3 mg ml⁻¹ doxycycline for 24 h. Then the cells were washed in phosphate buffered saline (PBS), gathered and snap frozen in liquid nitrogen and stored at -80 °C. We lysed the cell pellets by resuspension in HNN lysis buffer (50 mM HEPES pH 8, 150 mM NaCl, 50 mM NaF, 0.5% NP40, 400 mM Na₃VO₄, 1 mM PMSF and 0.2% protease inhibitors (Sigma)). The lysate was incubated on ice for 10 min and centrifuged at 18,000g for 30 min. The lysate was pooled, and 2 ml of lysate was used for each purification. We added 50 μ M of PFI-7, PFI-7N or DMSO, and 5 μ M of NB716 or DMSO to each sample. Treatments were done in triplicates. The samples were incubated at 4 °C for 1 h on a rotating wheel. Following addition of 100 μ l of Strep-Tactin Sepharose bead slurry (IBA Lifesciences, modified to be resistant to tryptic cleavage using 1,2-cyclohexanedione and sodium cyanoborohydride exactly as described in ref. 67), samples were incubated at 4 °C for 1 h on a rotating wheel. The samples were transferred to a 96-well 1 μ M glass filter plate (Pall Corporation). The lysate was filtered away, and the beads were washed twice with 1 ml

HNN lysis buffer without protease inhibitors and PMSF, twice with 1 ml of HNN lysis buffer without protease inhibitors, PMSF and NP40 and twice with 1 ml of 100 mM ammonium bicarbonate (ABC). The beads were transferred to a 10 kDa cutoff plate (Pall Corporation) in 100 mM ABC, and the plate was centrifuged for 40 min at 1,500g to remove the supernatant. The samples were resuspended in 8 M urea in 100 mM ABC, reduced with 5 mM tris(2-carboxyethyl)phosphine for 40 min at 37 °C and 800 rpm in a Thermomixer, alkylated with 40 mM iodoacetamide (IAA) for 30 min at 30 °C in the dark, at 800 rpm and digested with 1 μ g of trypsin (Promega) and 1 μ g of LysC (FUJIFILM Wako) overnight at 37 °C and 200 rpm. The supernatant was collected by centrifugation at 1,500g for 40 min. The beads were washed with 100 μ l of 100 mM ABC, and the wash was added to the collected supernatant. Digestion was stopped by adding 2% formic acid. The samples were desalted using C18 plates (Nest Group), dried and resuspended in 20 μ l water containing 0.1% formic acid. Then, 2 μ l of 10 \times iRT retention time standard (Biognosys) was added and 2 μ l of each sample were injected into a Orbitrap Eclipse Tribrid Mass Spectrometer (Thermo) coupled to an EASY-nLC 1000 System (Thermo). Peptides were separated on a 120 min gradient from 3 to 30% buffer B (95% ACN) on a 40 cm column packed with 1.9 μ m C18 resin (Dr. Maisch). To generate the spectral library, a pool of all samples was measured in data-dependent acquisition mode. The MS1 spectra were acquired in a scan range of 350–1,400 m/z with an Orbitrap resolution of 120,000. The normalized automatic gain control (AGC) target is set to 200% with a maximum injection time of 100 ms. The radio frequency (RF) lens was set to 30%. The targeted MS2 spectra are acquired for the top 20 peaks in the spectrum and fragmented with a higher-energy collisional disociation of 30%. The spectra are measured with an Orbitrap resolution of 30,000 with isolation windows of 1.2 m/z . The AGC target is set to 200% with a maximum injection time of 54 ms. We use a dynamic exclusion window of 60 s. The samples were then individually measured in data-independent acquisition mode. The MS1 spectra were acquired in a scan range of 350–1,400 m/z with an Orbitrap resolution of 120,000. The normalized AGC target was set to 200% with a maximum injection time of 100 ms. The RF lens was set to 30%. The targeted MS2 spectra are acquired for the desired masses with variable isolation windows (Supplementary Table 2) and fragmented with a higher-energy collisional disociation of 30%. The spectra were measured with an Orbitrap resolution of 30,000 with variable scan ranges. The AGC target is set to 400% with a maximum injection time of 54 ms. The RF lens was set to 30%. Hybrid libraries were generated using both the data-dependent acquisition and all data-independent acquisition runs, using the Pulsar search engine in Biognosys SpectroMine v.4. The standard settings were used with the digest type set to semispecific, and biotinylation was added as a variable modification. The runs were searched in Biognosys Spectronaut v.17 against the generated library. The precursor-level data were exported and further processed in protti v.0.6.0 in R v.4.2.1 (ref. 68). The data were normalized on the precursor level, and protein abundance was calculated based on at least three precursor intensities within each sample. The differential abundance was calculated and significance was determined across the triplicates using a moderated *t*-test with multiple testing correction using the method of Benjamini–Hochberg. We consider proteins to change significantly if the log₂(fold change) is below -1.0, and the adjusted *P* values are below 0.05.

Proximity-dependent biotinylation (BioID2)

For biotinylation experiments, three (BioID2 experiment no. 1 (BE1): DMSO versus MG132) or two (BioID2 experiment no. 2 (BE2): PFI-7 treatments) 15 cm plates of each inducible HeLa cell lines were grown to 85–95% confluence and induced with 1 μ g ml⁻¹ doxycycline. Four hours later, cells were supplemented with 50 μ M filter-sterilized biotin. For BE1, cells were also treated with 2 μ M MG132 or equivalent volume DMSO, or for BE2, 2 μ M MG132 and 10 μ M PFI-7 or equivalent volume DMSO. Twenty-four hours later, cells were washed thoroughly

in PBS, collected and pellets were flash frozen and stored at -80°C . Cell pellets were lysed in 1,300 μl RIPA lysis buffer on ice for 30 min with vortexing every 5 min (0.1% SDS, 0.5% sodium deoxycholate, 1% NP-40, 50 mM Tris-HCl, 150 mM NaCl, supplemented with benzonase nuclease (Sigma-Aldrich, cat. no. E1014) and protease inhibitors 0.2 mM PMSF, 1 mM DTT, 1 g ml^{-1} leupeptin, 10 g ml^{-1} aprotinin, 1 g ml^{-1} pepstatin (inhibitors obtained from BioShop). Cell extracts were then sonicated using a Fisher Scientific Sonic Dismembrator, model 100; 30 \times 1 s pulses at power level 2. Lysates were centrifuged at 17,968g 4°C for 30 min and quantified using 660 nm protein quantitation assay (Thermo, cat. nos. 22660 and 22663). A volume corresponding to 1.5 mg protein extract was incubated overnight with 50 μl of Dynabeads (MyOne Streptavidin C1; Invitrogen). Protein-bound beads were collected and washed once with Strep-biotin wash buffer (50 mM Tris-HCl pH 8, 1% SDS (w/v), 150 mM NaCl) at room temperature, rotating for 5 min. Beads were then washed twice with RIPA lysis buffer, followed by three washes in TAP lysis buffer (10% glycerol, 0.1% NP-40, 2 mM EDTA pH 8, 50 mM HEPES pH 7.9, 100 mM KCl). Finally, beads were washed three times using 50 mM NH_4HCO_3 (ABC) pH 8.0 solution before resuspension in ABC solution. Next, protein-bound beads were digested with 0.2 μg of mass spectrometry-grade Lysyl Endopeptidase (LysC) (125-05061, Wako Pure Chemical Ind.) at 37°C for 2 h before digestion overnight with 1 μg of trypsin/LysC mix (V5071, Promega) at 37°C . The released peptides were then transferred over to a new tube and a 4 h digest using 0.5 μg mass spectrometry-grade trypsin (cat. no. V5111, Promega) at 37°C for 4 h was conducted. Reactions were then acidified to a final concentration of 1% TFA and spun at maximum speed. The supernatant was then applied to Pierce C18 Spin Tips, cat. no. 4850 for desalting following the manufacturer's protocol. The eluted peptides were speed vacuumed to near dryness then resuspended in 20 μl of 0.1% formic acid. A volume corresponding to 500 ng peptides, as determined by bicinchoninic acid assay was then injected onto a Waters M-Class nanoAcuity high-performance liquid chromatography system (Waters) coupled to an electrospray ionization Orbitrap mass spectrometer (Q Exactive plus, ThermoFisher Scientific). Buffer A consisted of mass spectrometry-grade water with 0.1% formic acid and buffer B consisted of acetonitrile with 0.1% formic acid (ThermoFisher Scientific). All samples were trapped for 5 min at a flow rate of 5 $\mu\text{l min}^{-1}$ using 99% buffer A and 1% buffer B on a Symmetry BEH C18 Trapping Column (5 mm, 180 \times 20 mm, Waters). Peptides were separated using a Peptide BEH C18 Column (130 Å, 1.7 mm, 75 \times 250 mm) operating at a flow rate of 300 nl min^{-1} at 35°C (Waters). Samples were separated using a nonlinear gradient consisting of 1–7% buffer B over 1 min, 7–23% buffer B over 59 min and 23–35% buffer B over 20 min, before increasing to 98% buffer B and washing. Full MS spectra were acquired in positive mode at $R = 70,000$ in the 400–1,500 m/z mass range, 250 ms injection time, 3×10^6 ACG target. The top 12 peptides were selected for higher-energy collisional dissociation at $R = 17,500$ (ACG target, 2 $\times 10^5$; injection time, 64 ms; loop count, 12; isolation width, 1.2 m/z ; isolation offset, 0.5 m/z ; normalized collision energy, 25; intensity threshold, 3.1×10^4 ; charge exclusion, unassigned, 1, 7, 8, >8; dynamic exclusion enabled, 30 s). For BE1, data were searched using MaxQuant v.1.5.8.3 using the Human UniProt database (reviewed only; updated May 2017 with 42,183 entries). Missed cleavages were set to 3, cysteine carbamidomethylation was set as a fixed modification and oxidation (*M*), N-terminal acetylation (protein) and deamidation (NQ) were set as variable modifications (maximum number of modifications per peptide was five) and peptide length ≥ 7 . All other parameters were left at default. For BE2, data was searched using PEAKS Studio v.8.5 (Bioinformatics Solutions Inc.) using the Human UniProt database (reviewed only; updated November 2019). Missed cleavages was set to three and semispecific cleavage was enabled. Parent mass error tolerance was set to 20 ppm, fragment mass error tolerance was set to 0.8 Da. Protein and peptide false discovery rate (FDR) was set to 1%. Cysteine carbamidomethylation was set as a fixed modification while oxidation (*M*) and N-terminal deamidation

(NQ) were set as variable modifications (maximum number of modifications per peptide was five). Proteins were identified using a minimum of two unique peptide(s) with the FDR set to 1%. Spectral counts data were formatted for SAINTexpress analysis, a computational algorithm integrated into the REPRINT website (<https://reprint-apms.org/>). Analyzed data were visualized in cytoscape⁶⁹. Gene ontology terms were identified using the package goseq (v.1.42.0) in R (v.4.0.3) with *P* values adjusted using the Benjamini–Hochberg method and a threshold of adjusted *P* < 0.05. Comparison between GID4 interactome and the human cell map database was done at <https://humancellmap.org/> against the entire database³³.

Global quantitative proteomics using label-free LC–MS/MS

For proteome sample preparation, MG132-treated samples were the same extracts used in BE2. For non-MG132 samples, a separate 10 cm cell dish grown in parallel with BE2 treatments and replicates was treated with an equivalent volume of DMSO and collected and lysed at the same time as the BE2 extracts. Twenty-five microgram of protein lysate was reduced in 10 mM DTT for 25 min, alkylated in 10 mM iodoacetamide for 25 min in the dark, followed by methanol precipitation. The protein pellet was resuspended in 50 mM ABC and subjected to a sequential digest first with 250 ng of LysC (cat. no. 125-05061, Wako Pure Chemical Ind., Ltd) for 4 h, then 500 ng of trypsin/LysC (cat. no. V5071, Promega) for 16 h, followed by 500 ng of trypsin (cat. no. V5111, Promega) for an additional 4 h. Digestions were incubated at 37°C at 600 rpm on a Thermomixer C (cat. no. 2231000667, Eppendorf). After the last digestion, samples were acidified with 10% formic acid to pH 3–4, centrifuged at 14,000g for 5 min, then peptides desalted using Pierce C18 Spin Tips (cat. no. 84850). Samples were then dried in a speed vacuum, resuspended in 0.1% formic acid and quantified by bicinchoninic acid assay. Approximately 500 ng of peptide sample was injected onto a Waters M-Class nanoAcuity ultrahigh-performance liquid chromatography system (Waters) coupled to an electrospray ionization Orbitrap mass spectrometer (Q Exactive plus, ThermoFisher Scientific). Samples were trapped for 5 min at a flow rate of 5 $\mu\text{l min}^{-1}$ using 99% buffer A and 1% buffer B on a Symmetry BEH C18 Trapping Column (5 mm, 180 \times 20 mm, Waters). Peptides were separated using a Peptide BEH C18 Column (130 Å, 1.7 mm, 75 \times 250 mm) operating at a flow rate of 300 nl min^{-1} at 35°C (Waters). Proteome samples were separated using a nonlinear gradient consisting of 1–7% buffer B over 1 min, 7–23% buffer B over 179 min and 23–35% buffer B over 60 min, before increasing to 98% buffer B and washing. Full MS spectra were acquired in positive mode at $R = 70,000$ in the 400–1,500 m/z mass range, 250 ms injection time, 3×10^6 ACG target. The top 12 peptides were selected for higher-energy collisional dissociation at $R = 17,500$ (ACG target, 2 $\times 10^5$; injection time, 64 ms; loop count, 12; isolation width, 1.2 m/z ; isolation offset, 0.5 m/z ; normalized collision energy, 25; intensity threshold, 3.1×10^4 ; charge exclusion, unassigned, 1, 7, 8, >8; dynamic exclusion enabled, 30 s). All MS raw files were searched in MaxQuant v.1.5.8.3 using the Human Uniprot database (reviewed only; updated July 2020). Missed cleavages were set to 3, cysteine carbamidomethylation was set as a fixed modification and oxidation (*M*), N-terminal acetylation (protein) and deamidation (NQ) were set as variable modifications (maximum number of modifications per peptide was five) and peptide length ≥ 6 . Protein and peptide FDR was left to 0.01 (1%) and decoy database was set to revert. Match between runs was enabled and all other parameters left at default. Protein groups were loaded into R (v.4.0.3, R Core Team (2020), <https://www.R-project.org/>) and reverse, potential contaminant or proteins quantified in less than two out of four replicates of at least one condition were removed. Uniprot IDs were matched to gene symbols using biomaRt⁷⁰ (v.2.46.3) and UniProt. Mixed imputation was performed using DEP⁷¹ (v.1.12.0) as described in the package documentation. Testing for protein differential abundance was done using DEP with an adjusted *P* threshold of <0.05, fold change >1.5. Heatmap and hierarchical clustering was done using pheatmap

(R. Kolde (2019), <https://CRAN.R-project.org/package=heatmapr>, v.1.0.12), UMAP clustering was done using UMAP (v.0.2.7.0, T. Konopka (2020), <https://CRAN.R-project.org/package=umap>). PCA was done using the stats package function prcomp (R v.4.0.3).

Immunoprecipitation

RanBPM immunoprecipitation in whole-cell extracts of BioID2-GID4 HeLa transfected cells was conducted exactly as previously described for RanBPM affinity purification mass spectrometry using DMP-crosslinked RanBPM antibody to dynabeads with 0.5 mg of protein extract, 5 µg of RanBPM antibody (F1, sc-271727, Santa Cruz Biotechnology) and 20 µl of Dynabeads Protein G (10004D, Invitrogen, Life Technologies)²⁵. Immunoprecipitation of HA-BioID2-GID4 was conducted with 5 µg of HA antibody (HA-7, H9658, Sigma-Aldrich), 20 µl of Dynabeads Protein G and 0.5 mg of precleared protein extract adjusted to 0.25% NP-40. Antibody and extract rotated overnight at 4 °C then incubated for 1 h at 4 °C with beads, washed three times in lysis buffer and resuspended in SDS loading buffer. FLAG-GID4 immunoprecipitation in 293T GID4 expressing cells was done in the same lysis and binding conditions as HA immunoprecipitation but with 1 mg of protein extract and 20 µl of Anti-FLAG M2 Magnetic beads (cat. no. M8823, Sigma-Aldrich). Cells were treated with 1 µM PFI-7N or PFI-7 for 24 h, and 10 µM PFI-7N or PFI-7 was also added to immunoprecipitation samples before incubation with beads. Precipitated proteins were then eluted with 500 µg ml⁻¹ FLAG peptide for 2 h at 4 °C.

Fluorescence microscopy

HeLa BioID2-GID4 or BioID2 alone cells were seeded onto coverslips, fixed using 4% paraformaldehyde 10 min at 4 °C, then permeabilized with 0.5% Triton X-100 for 15 min at room temperature. Cells were blocked in 5% FBS then incubated overnight at 4 °C with primary mouse antibody against HA (H9658, Sigma-Aldrich, 1:1,000) and then with secondary Alexa 488 antibody against mouse (Invitrogen, Life Technologies, 1:1,000). The coverslips were mounted using ProLong Gold containing 4,6-diamidino-2-phenylindole (DAPI) (Invitrogen). Cell images were taken with an Olympus BX51 microscope at ×40 magnification and Image-Pro Plus (v.5.0) software (Media Cybernetics, Inc.). For microscopy of FLAG-tagged GID4, 2 × 10⁵ U2OS cells were seeded in 12-well plates with 1 µg ml⁻¹ of doxycycline with 10 µM PFI-7 or DMSO control for 24 h. Cells were fixed with 2% paraformaldehyde in 1× PBS for 10 min and permeabilized with 0.1% Triton X-100 in 1× PBS for 5 min at room temperature. Samples were then blocked with 2% bovine serum albumin (Sigma) in PBS-T (1× PBS and 0.1% Tween-20) for 1 h at room temperature and incubated overnight at 4 °C with primary antibody staining for FLAG (Sigma, cat. no. F1804, 1:500) and DDX50 (Protein-tech, cat. no. 10358-I-AP, 1:400). Cells were washed three times with 1× PBS, followed by staining with fluorescent antimouse (Alexa Fluor 488 Conjugate; Cell Signaling Technologies, cat. no. 44085; 1:400) and antirabbit (Alexa Fluor 594 Conjugate; Cell Signaling Technologies, cat. no. 8889; 1:400) for 1 h at room temperature. Unbound secondary antibodies were removed by three 1× PBS washes and coverslips were mounted onto slides using with Fluoroshield with DAPI (Sigma, cat. no. F6057). Images were acquired with Quorum Spinning Disk Confocal Microscope equipped with 405, 491, 561 and 642 nm lasers (Zeiss) and processed with Volocity software (Perkin Elmer) and ImageJ.

Western blotting

For immunoblotting of experiments relating to BioID2-GID4, extracts were resolved by SDS-PAGE (10%) before transfer onto a polyvinylidene difluoride (PVDF) membrane and blocking in 5% skim milk in TBST solution (tris-buffered saline with Tween). Membranes were hybridized overnight with the following antibodies: mouse anti-HA (cat. no. H3663, Sigma-Aldrich, 1:5,000), RanBPM (5 M, cat. no. 71-001, Bioacademia, 1:2,000), Vinculin (cat. no. E1E9V, Cell Signaling Technology, 1:10,000), SAP62 (1:1,000; A-3, cat. no. sc-390444, Santa Cruz

Biotechnology), Muskelin (C-12, cat. no. sc-398956, Santa Cruz Biotechnology, 1:1,000), ARMC8 (E-1, cat. no. sc-365307; Santa Cruz Biotechnology, 1:500), WDR26 (cat. no. ab85962, Abcam, 1:2,000), RMND5A (1:2,000; custom-made antibody from Yenzyyme Antibodies) and MAEA (cat. no. AF7288, R&D Systems, 1:250). Biotinylated proteins were detected similarly: following transfer, PVDF membranes were blocked overnight in 0.5% fish gelatin in TBST solution and incubated for 1 h with horse radish peroxidase-conjugated streptavidin (Pierce High Sensitivity Streptavidin-HRP, ThermoFisher Scientific, 1:20,000). Blots were imaged using the ClarityWestern ECL substrate (Bio-Rad) and the Molecular Imager ChemiDocTM XRS system (Bio-Rad) with Image Lab (v.6.0.1.). For immunoblotting of experiments relating to FLAG-GID4 (DDX21/50 coimmunoprecipitation with PFI-7, HMGCS1 regulation), samples were boiled in SDS loading buffer before western blotting using the NuPAGE electrophoresis and transfer system (Invitrogen) and near-infrared detection for DDX21 and DDX50 (Proteintech, cat. no. 10358-1-AP, 1:500 (Supplementary Fig. 2), FLAG (SIGMA, cat. no. F1804, 1:5,000), HMGCS1 (Cell Signaling Technology, cat. no. D1Q9D, 1:3,000) and Actin (Cell Signaling Technology, cat. no. 3700S, 1:10,000). Immunoblots were imaged on a Li-Cor Odyssey CLx and quantified in Image Studio Lite v.5.2.5 (Li-Cor Biosciences).

Reporting summary

Further information on research design is available in the Nature Portfolio Reporting Summary linked to this article.

Data availability

The mass spectrometry data have been deposited to the ProteomeXchange Consortium via the PRIDE partner repository with the dataset identifier [PXD038487](#). The mass spectrometry data of the chemoproteomics experiment have been deposited to the ProteomeXchange Consortium via the PRIDE partner repository with the dataset identifier [PXD044977](#). The structure of PFI-7 bound to GID4 was deposited to the PDB with accession number [7SLZ](#). Source data are provided with this paper.

Code availability

R scripts for analysis of proteomics data are freely available at https://github.com/d0minic0/GID4_analysis.

References

57. Kabsch, W. XDS. *Acta Crystallogr. Sect. D* **66**, 125–132 (2010).
58. Otwinowski, Z. & Minor, W. Processing of X-ray diffraction data collected in oscillation mode. *Methods Enzymol.* **276**, 307–326 (1997).
59. McCoy, A. J. et al. Phaser crystallographic software. *J. Appl. Crystallogr.* **40**, 658–674 (2007).
60. Murshudov, G. N., Vagin, A. A. & Dodson, E. J. Refinement of macromolecular structures by the maximum-likelihood method. *Acta Crystallogr. Sec. D* **53**, 240–255 (1997).
61. Bricogne, G. et al. BUSTER v.2.9 (Global Phasing Ltd, 2010).
62. Smart, O. S. et al. GRADE v.1.102 (Global Phasing Ltd, 2011).
63. Emsley, P. & Cowtan, K. Coot: model-building tools for molecular graphics. *Acta Crystallogr. D. Biol. Crystallogr.* **60**, 2126–2132 (2004).
64. Williams, C. J. et al. MolProbity: more and better reference data for improved all-atom structure validation. *Protein Sci.* **27**, 293–315 (2018).
65. Gräslund, S., Savitsky, P. & Müller-Knapp, S. In vivo biotinylation of antigens in *E. coli*. *Methods Mol. Biol.* **1586**, 337–344 (2017).
66. Schwalm, M. P. et al. A toolbox for the generation of chemical probes for baculovirus IAP repeat containing proteins. *Front Cell Dev. Biol.* **10**, 886537 (2022).
67. Rafiee, M.-R. et al. Protease-resistant streptavidin for interaction proteomics. *Mol. Syst. Biol.* **16**, e9370 (2020).

68. Quast, J. P., Schuster, D. & Picotti, P. protti: an R package for comprehensive data analysis of peptide- and protein-centric bottom-up proteomics data. *Bioinformatics Adv.* **2**, vbab041 (2021).
69. Shannon, P. et al. Cytoscape: a software environment for integrated models of biomolecular interaction networks. *Genome Res.* **13**, 2498–2504 (2003).
70. Durinck, S., Spellman, P. T., Birney, E. & Huber, W. Mapping identifiers for the integration of genomic datasets with the R/Bioconductor package biomaRt. *Nat. Protoc.* **4**, 1184–1191 (2009).
71. Zhang, X. et al. Proteome-wide identification of ubiquitin interactions using UbIA-MS. *Nat. Protoc.* **13**, 530–550 (2018).

Acknowledgements

This work was supported by Mitacs Elevate Postdoctoral Fellowship to D.D.G.O., funding from the Canadian Institutes for Health Research (grant nos. MOP-142414 and PJT-169101 to C.S.-P.; FDN154328 to C.H.A.), Natural Sciences and Engineering Research Council of Canada grant nos. RGPIN-2021-02728 to J.M. and RGPIN-2021-03435 to D.B.-L. and a Cancer Research Society grant no. 25418 to D.B.-L. M.P.S. is funded by the Deutsche Forschungsgemeinschaft CRC1430 (Project ID 424228829). V.R. and M.G. have received support from the EU/EFPIA/OICR/McGill/KTH/Diamond Innovative Medicines Initiative 2 Joint Undertaking (EUbOPEN grant no. 875510). We thank M. Robers and K. Riching from Promega for advising on the NanoBRET and target engagement assays. This research used resources of the Advanced Photon Source, a US Department of Energy (DOE) Office of Science user facility operated for the DOE Office of Science by Argonne National Laboratory under contract no. DE-AC02-06CH11357. Mass spectrometry analyses were performed on equipment funded by a grant from the Canada Foundation for Innovation to G.A.L. The Structural Genomics Consortium is a registered charity (no. 1097737) that receives funds from Bayer AG, Boehringer Ingelheim, Bristol Myers Squibb, Genentech, Genome Canada through the Ontario Genomics Institute (OGI-196), EU/EFPIA/OICR/McGill/KTH/Diamond Innovative Medicines Initiative 2 Joint Undertaking (EUbOPEN grant no. 875510), Janssen, Merck KGaA (also known as EMD in Canada and the United States), Pfizer and Takeda.

Author contributions

M.E.R.M., D.D.G.O., X.W., E.C.A., M.M.S., R.A.C.M., P.L., D.B.-L. and C.S.-P. designed and performed cellular experiments. M.E.R.M. and G.A.L. designed and performed proteomic experiments. D.D.G.O. conducted proteomic data analysis. V.R. and M.G. designed, performed and analyzed the chemoproteomic experiments. N.B., M.P.S. and S.K. designed and performed GID4-tracer NanoBRET assay and generated NB716. A.K.Y. and M.V. designed and performed biophysical experiments. M.F.C., M.S.D., J.L., J.I.M., T.N.O., D.R.O., C.S. and F.W. designed and synthesized compounds. X.S., C.D., J.M. and A.D. performed crystallography studies and solved structures. C.H.A., M.V., J.M., D.B.-L., M.S., G.A.L. and C.S.-P. supervised research. C.H.A., D.B.-L., C.S.-P. and J.M. provided funding. C.H.A., D.B.-L., M.E.R.M. and D.D.G.O. wrote the manuscript.

Competing interests

M.F.C., M.S.D., J.L., J.I.M., T.N.O., C.S., F.W. and D.R.O. are or were employees of Pfizer and some of the authors are shareholders in Pfizer Inc. After submission, D.D.G.O. became an employee of Amphista Therapeutics, a company that is developing targeted protein degradation therapeutic platforms. The remaining authors declare no competing interests.

Additional information

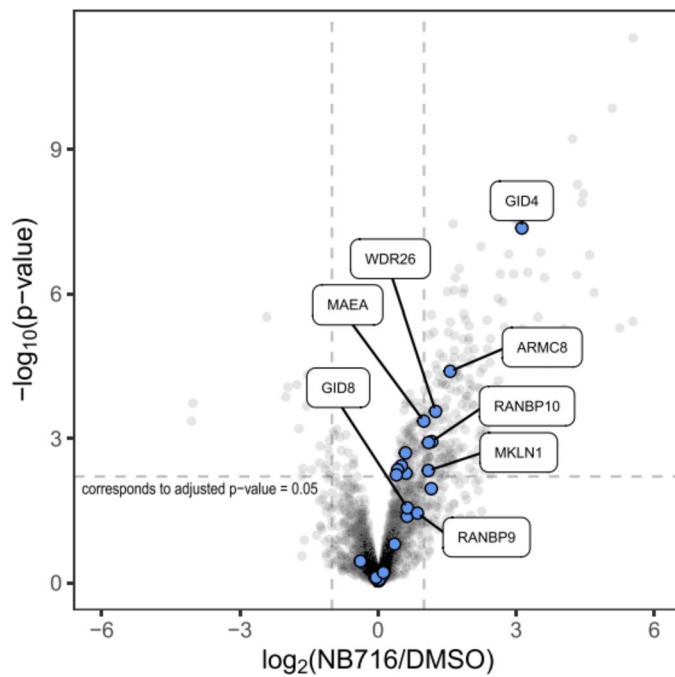
Extended data is available for this paper at <https://doi.org/10.1038/s41589-024-01618-0>.

Supplementary information The online version contains supplementary material available at <https://doi.org/10.1038/s41589-024-01618-0>.

Correspondence and requests for materials should be addressed to Cheryl H. Arrowsmith.

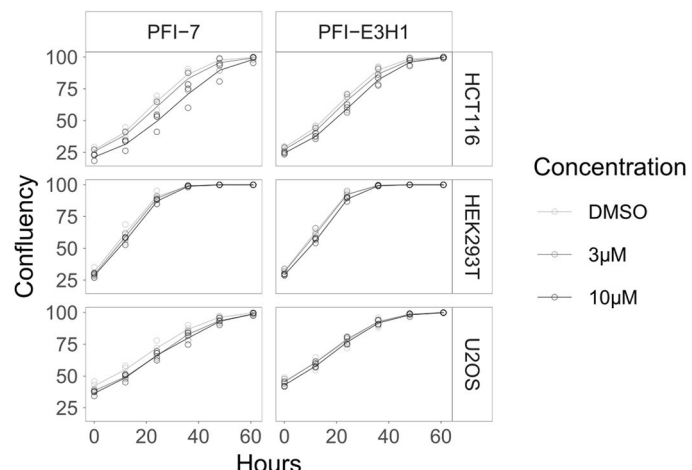
Peer review information *Nature Chemical Biology* thanks Nico Dissmeyer, Chao Xu and the other, anonymous, reviewer(s) for their contribution to the peer review of this work.

Reprints and permissions information is available at www.nature.com/reprints.

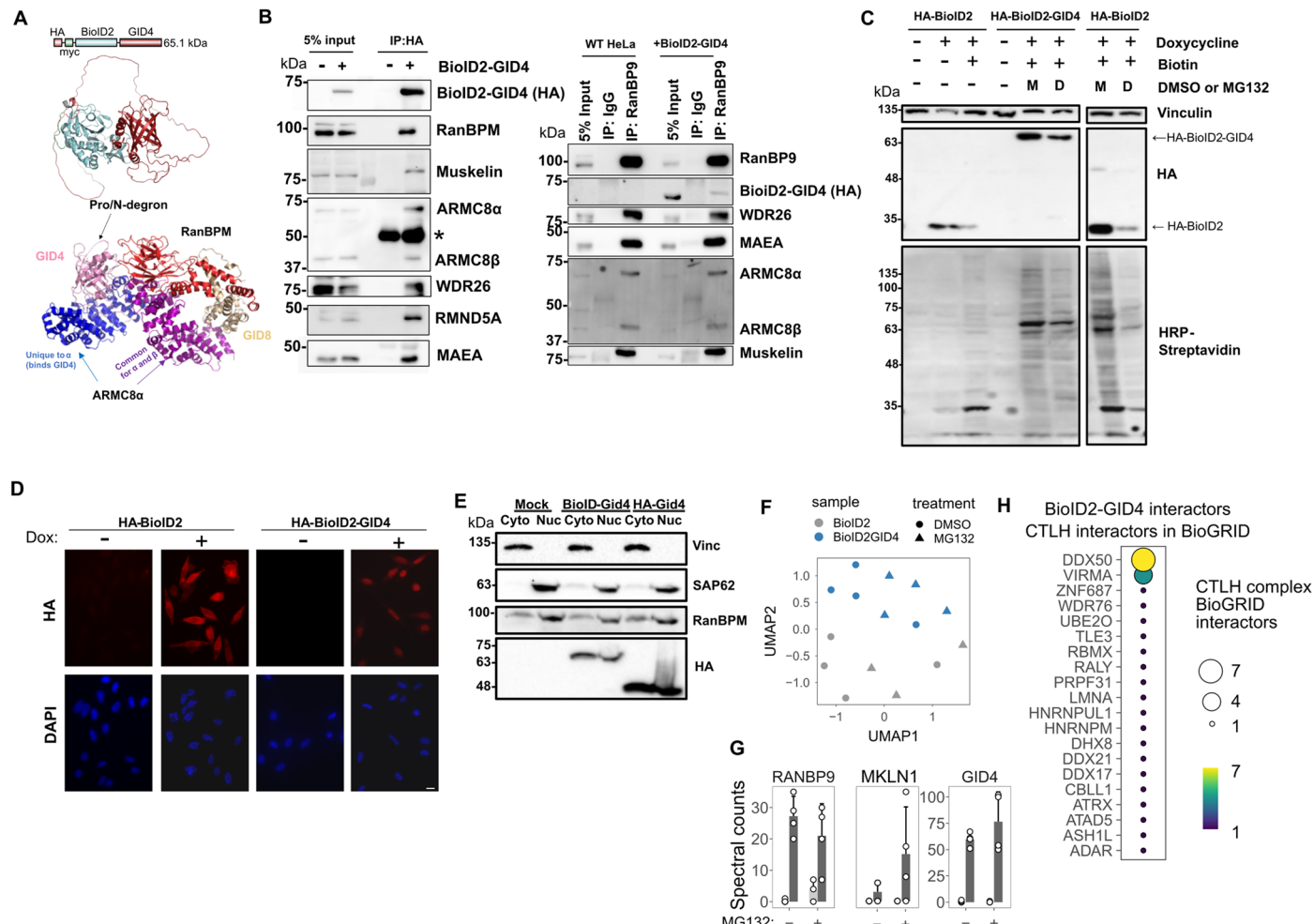


Extended Data Fig. 1 | Enrichment profiling of NB716. The volcano plot shows the proteins enriched by streptavidin affinity purification in the presence of NB716. GID4 is among the most highly enriched proteins. Many known interaction partners shown in blue are also highly enriched. The differential

abundance was calculated and significance was determined using a two-tailed moderated t-test with multiple testing correction using the method of Benjamini-Hochberg. Data are from three independent experiments ($n = 3$).

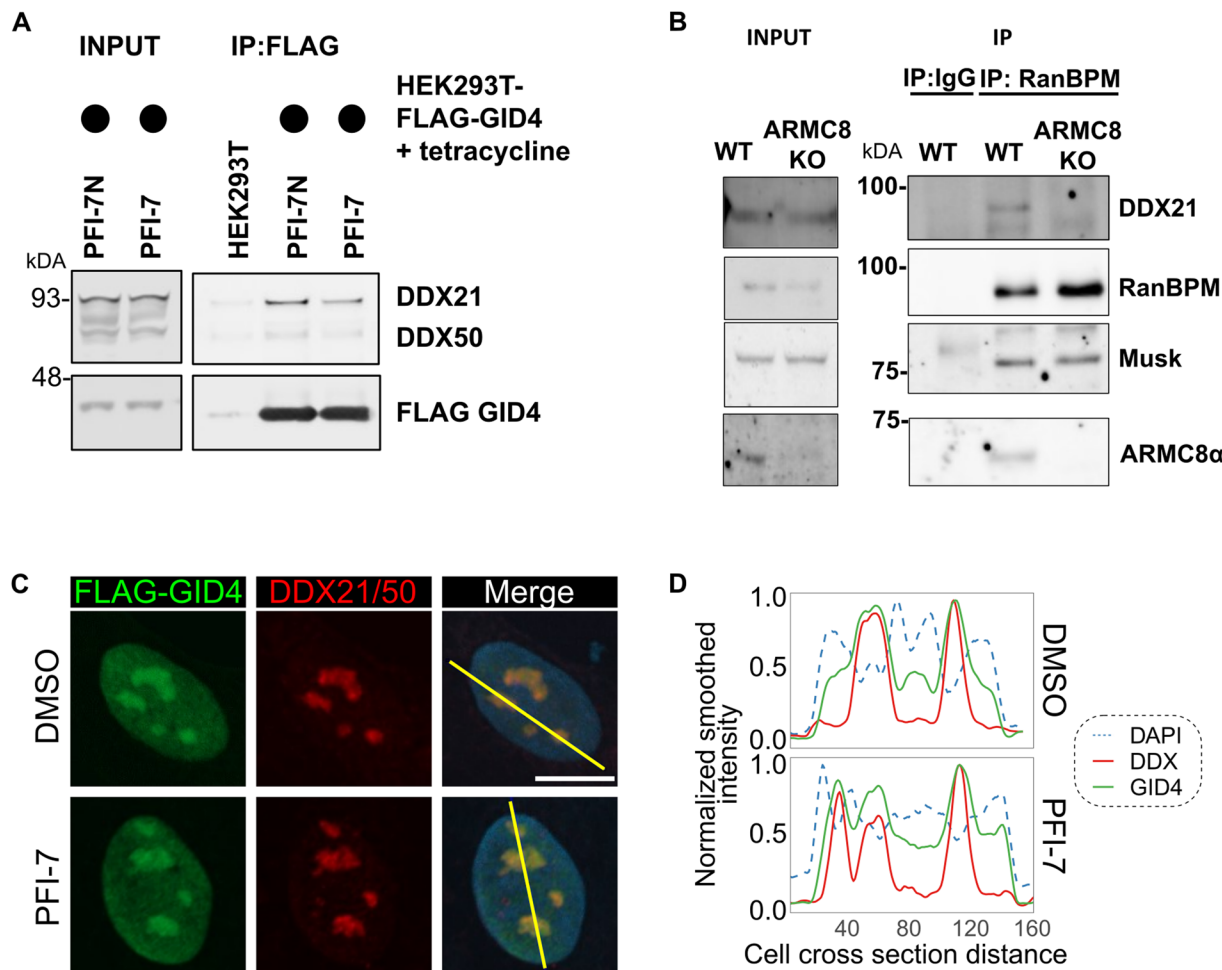


Extended Data Fig. 2 | Cytotoxic profile of PFI-7. Cell growth curves for HCT116, HEK293T and U2OS cells treated with increasing concentrations of PFI-7 or PFI-E3H1 are shown over three days. Data are from three independent experiments ($n = 3$).



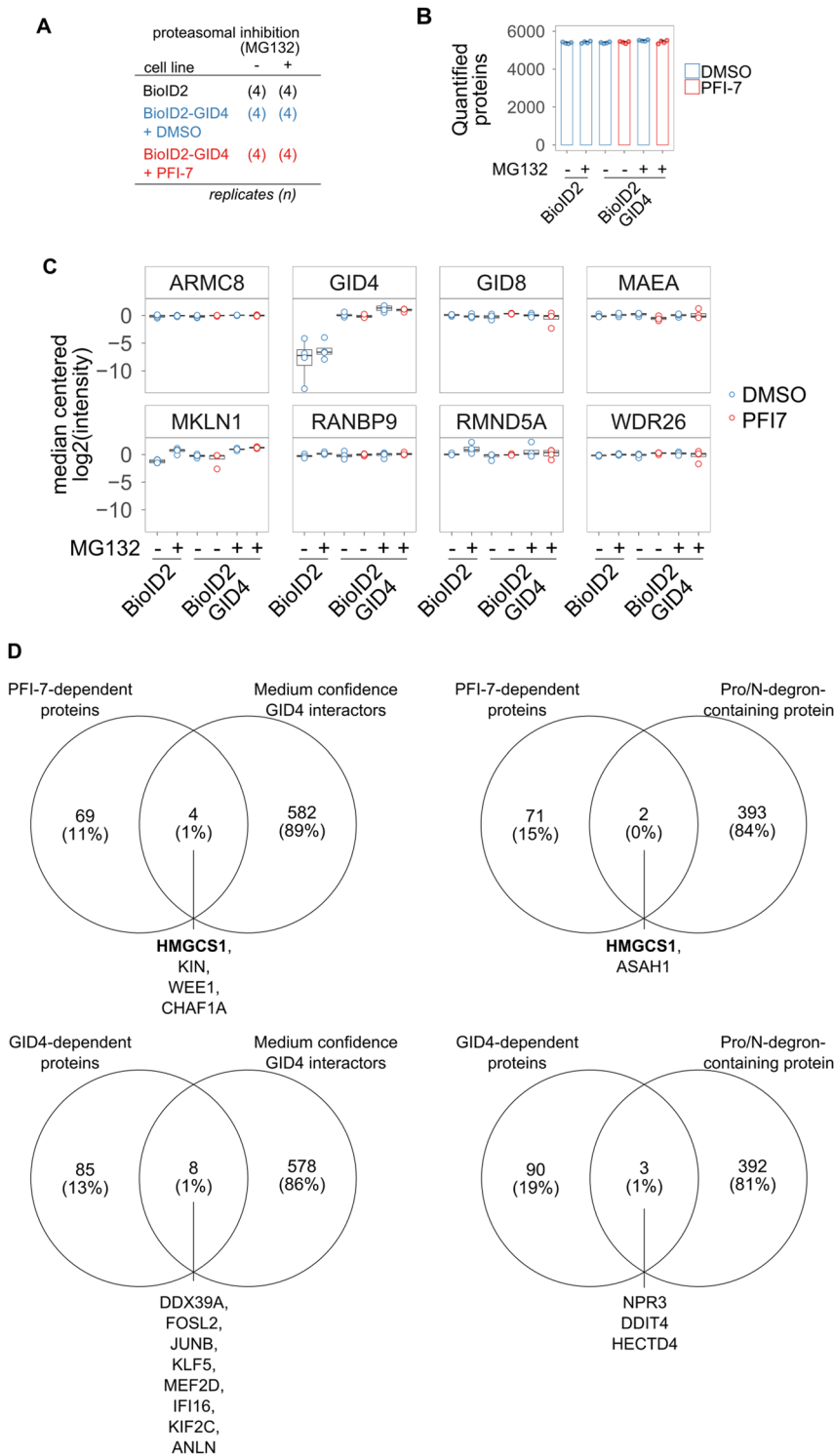
Extended Data Fig. 3 | Characterization of GID4-BioID2 cell line.
a) Upper, schematic and AlphaFold2 predicted structure of GID4-BioID2 fusion protein. Lower, partial CTLH complex structure (PDB 7NSC) showing GID4 C-terminal anchor interacting with ARMC8α (Ref. 31 – Sherpa et al, 2021).
b) Immunoprecipitation experiments performed in HeLa cells. Left, HA-pull down of BioID2-GID4 fusion protein with immunoblotting to detect CTLH complex members. Right, immunoprecipitation of RanBP9 with immunoblotting to detect BioID2-GID4 (HA) and other CTLH complex members, * = heavy chain. Data are from one experiment ($n = 1$). **c)** Immunoblotting to detect BioID2-GID4 or BioID2 alone after doxycycline induction (top). Bottom, streptavidin-based detection of biotinylated proteins. Representative blot shown from one of five independent experiments ($n = 5$). **d)** Immunofluorescence imaging of HA in BioID2 and BioID2-GID4-expressing HeLa cells. HA signal is shown in red, DAPI is shown in blue. Representative images are shown from one of three independent experiments ($n = 3$). Scale bar: 20 μ m. **e)** Nuclear and cytoplasmic fractionation of HeLa cells expressing BioID2-GID4 or HA-GID4 alone. Immunoblotting of

Vinculin, SAP62, RanBP9, and HA is shown. Representative blot shown from one of two independent experiments ($n = 23$). **f)** Uniform Manifold Approximation and Projection (UMAP) analysis of proximity-dependent biotinylation samples. BioID2 and BioID2-GID4 cells are shown in gray and blue, respectively. MG132-treated samples are indicated as triangles, and samples treated with vehicle (DMSO) are shown as circles. UMAP was done on 196 high confidence GID4 interacting proteins (MG132 SP > 0.9). Data are from three independent experiments ($n = 3$, BioID2 + MG132) or four independent experiments ($n = 4$, BioID2 + DMSO, BioID2-GID4 + DMSO, BioID2-GID4 + MG132). **g)** Spectral counts of CTLH complex members detected in BioID2-GID4. Bar height represents mean and error bars indicate standard deviation. Data are from three independent experiments ($n = 3$, BioID2 + MG132) or four independent experiments ($n = 4$, BioID2 + DMSO, BioID2-GID4 + DMSO, BioID2-GID4 + MG132). **h)** Overlap between high confidence GID4 interactors and interactors of the CTLH complex present in the BioGRID database.



Extended Data Fig. 4 | DDX50 and DDX21 association with GID4 and CTLH complex. **a**) Immunoprecipitation of FLAG-GID4 in HEK293T cells expressing FLAG-GID4 treated with 1 μM PFI-7N or PFI-7 for 24 hours. Data are from two experiments ($n = 2$). **b**) Immunoprecipitation of RanBP9 in wild type (WT) and ARMC8 knock-out (ARMC8 KO) HeLa cells. Immunoblotting was done for DDX21/50, FLAG, RanBP9, Muskelin and ARMC8α. Data are from one experiment ($n = 1$). **c**) Confocal imaging analysis of U2OS cells transduced with a doxycycline inducible lentiviral expression vector coding for N terminally FLAG-tagged GID4.

FLAG-GID4 expression was induced for 24 h and is shown in green, DDX21/50 (antibody recognizes both endogenous proteins) is shown in red, and DAPI is shown in blue. Scale bar represents 15 μm. Representative images are shown from four independent experiments. **d**) Quantification of fluorescence signal intensity over a cross section of cell nuclei. A rolling average with a window size of 8 was used to smooth data and maximum intensities were scaled to 1. One cell from each condition was quantified from one of four independent experiments.



Extended Data Fig. 5 | Proteomic samples used and overlap with other datasets. **a)** Proteomics samples with number of replicates and treatment conditions shown. Data are from four independent experiments ($n = 4$). These replicate numbers apply to all panels of the figure. **b)** Number of quantified proteins detected in each sample. Bar height represents mean values and error bars indicate standard deviation. $N = 4$ independent experiments. **c)** Protein abundances of CTLH complex members. Median-centered log₂ intensities are shown, with blue dots indicating DMSO-treated samples and PFI-7-treated samples shown in red. Boxplot midline indicates median values, bounds of

the box indicate 25th and 75th percentiles, and maxima and minima indicate the largest point above or below 1.5 * interquartile range. $N = 4$ independent experiments. **d)** Overlap between proteins significantly changed after PFI-7 treatment or GID4 overexpression and medium confidence GID4 interactors ($SP > 0.6$ in any condition), left. Right, PFI-7-dependent and GID4-dependent proteins overlap with Pro/N-degron-containing proteins. SP scores derived from $N = 3$ independent experiments in BioID2-GID4 data, protein abundance change significance derived from $n = 4$ independent expression proteomics experiments.

Reporting Summary

Nature Portfolio wishes to improve the reproducibility of the work that we publish. This form provides structure for consistency and transparency in reporting. For further information on Nature Portfolio policies, see our [Editorial Policies](#) and the [Editorial Policy Checklist](#).

Statistics

For all statistical analyses, confirm that the following items are present in the figure legend, table legend, main text, or Methods section.

n/a Confirmed

- The exact sample size (n) for each experimental group/condition, given as a discrete number and unit of measurement
- A statement on whether measurements were taken from distinct samples or whether the same sample was measured repeatedly
- The statistical test(s) used AND whether they are one- or two-sided
Only common tests should be described solely by name; describe more complex techniques in the Methods section.
- A description of all covariates tested
- A description of any assumptions or corrections, such as tests of normality and adjustment for multiple comparisons
- A full description of the statistical parameters including central tendency (e.g. means) or other basic estimates (e.g. regression coefficient) AND variation (e.g. standard deviation) or associated estimates of uncertainty (e.g. confidence intervals)
- For null hypothesis testing, the test statistic (e.g. F , t , r) with confidence intervals, effect sizes, degrees of freedom and P value noted
Give P values as exact values whenever suitable.
- For Bayesian analysis, information on the choice of priors and Markov chain Monte Carlo settings
- For hierarchical and complex designs, identification of the appropriate level for tests and full reporting of outcomes
- Estimates of effect sizes (e.g. Cohen's d , Pearson's r), indicating how they were calculated

Our web collection on [statistics for biologists](#) contains articles on many of the points above.

Software and code

Policy information about [availability of computer code](#)

Data collection	a BioTek Synergy 4; Biacore T200 Evaluation Software 3.1; Image Studio Lite v5.2.5 (Li-Cor Biosciences); Volocity software (Perkin Elmer); ImageJ; Image-Pro Plus (v5.0) software (Media Cybernetics, Inc., Bethesda, MD, USA).
Data analysis	<p>Structure: The data were processed using XDS and the HKL-3000 suite respectively, and the structure was solved by molecular methods using PDB 6WZZ as a search template with the program PHASER (2.8.3). REFMAC (5.8.0158) and BUSTER (2.10.3) were used for structure refinement. Geometry restraints for the compound refinement were prepared with by GRADE (v1.102) developed at Global Phasing Ltd. Graphics program COOT (version 0.8.9.2) was used for model building and visualization. Molprobity (4.02b-467) was used for structure validation.</p> <p>FP data were visualized using GraphPad Prism software 8.0 (La Jolla, CA).</p> <p>Competitive displacement data were graphed using GraphPad Prism 9 software using a normalized 3-parameter curve fit with the following equation: $Y=100/(1+10^{(X-\text{LogIC50})})$.</p> <p>For chemoproteomics: Pulsar search engine in Biognosys SpectroMine version 4. Biognosys Spectronaut version 17. The precursor-level data was exported and further processed in protti version 0.6.0 in R version 4.2.1.</p> <p>For BioID: data was searched using MaxQuant v1.5.8.3 or PEAKS Studio version 8.5 (Bioinformatics Solutions Inc.). Spectral counts data were formatted for SAINTexpress analysis (https://reprint-apms.org/). Analyzed data were visualized in cytoscape. GO terms were identified using the package goseq (1.42.0) in R (4.0.3)</p> <p>For global proteome analysis: All MS raw files were searched in MaxQuant version 1.5.8.3. Protein groups were loaded into R (4.0.3, R Core Team (2020), https://www.R-project.org/) and reverse, potential contaminant, or proteins quantified in less than two out of four replicates at least one condition were removed. Uniprot IDs were matched to gene symbols using biomaRt69 (2.46.3) and Uniprot. Mixed imputation was performed using DEP70 (1.12.0) as described in the package documentation. Testing for protein differential abundance was done using DEP with an adjusted p-value threshold of < 0.05, fold change > 1.5. Heatmap and hierarchical clustering was done using pheatmap (Raivo</p>

Kolde (2019), <https://CRAN.R-project.org/package=pheatmap>, 1.0.12), UMAP clustering was done using umap (0.2.7.0, Tomasz Konopka (2020), <https://CRAN.R-project.org/package=umap>). Principal Components Analysis was done using the stats package function prcomp (R 4.0.3).

R scripts for analysis of proteomics data are freely available at https://github.com/dominicO/GID4_analysis.

For manuscripts utilizing custom algorithms or software that are central to the research but not yet described in published literature, software must be made available to editors and reviewers. We strongly encourage code deposition in a community repository (e.g. GitHub). See the Nature Portfolio [guidelines for submitting code & software](#) for further information.

Data

Policy information about [availability of data](#)

All manuscripts must include a [data availability statement](#). This statement should provide the following information, where applicable:

- Accession codes, unique identifiers, or web links for publicly available datasets
- A description of any restrictions on data availability
- For clinical datasets or third party data, please ensure that the statement adheres to our [policy](#)

The mass spectrometry data have been deposited to the ProteomeXchange Consortium via the PRIDE partner repository with the dataset identifier PXD038487. The mass spectrometry data of the chemoproteomics experiment have been deposited to the ProteomeXchange Consortium via the PRIDE partner repository with the dataset identifier PXD044977. The structure of PFI-7 bound to GID4 was deposited to the Protein Data Bank with accession number 7SLZ. BioID experiment 1 used Human Uniprot database (reviewed only; updated May 2017). BioID experiment 2 used Human Uniprot database (reviewed only; updated November 2019). Whole proteome analysis used Human Uniprot database (reviewed only; updated July 2020).

Research involving human participants, their data, or biological material

Policy information about studies with [human participants or human data](#). See also policy information about [sex, gender \(identity/presentation\), and sexual orientation](#) and [race, ethnicity and racism](#).

Reporting on sex and gender

N/A

Reporting on race, ethnicity, or other socially relevant groupings

N/A

Population characteristics

N/A

Recruitment

N/A

Ethics oversight

N/A

Note that full information on the approval of the study protocol must also be provided in the manuscript.

Field-specific reporting

Please select the one below that is the best fit for your research. If you are not sure, read the appropriate sections before making your selection.

Life sciences Behavioural & social sciences Ecological, evolutionary & environmental sciences

For a reference copy of the document with all sections, see nature.com/documents/nr-reporting-summary-flat.pdf

Life sciences study design

All studies must disclose on these points even when the disclosure is negative.

Sample size

Based on previous experience from similar studies (PMID: 31848333, 34782742, 34383978) and pilot studies, experiments were performed at least 2-3 times to confirm reproducibility. Sample sizes are described in Methods and figure legends.

Data exclusions

None.

Replication

All attempts at replication were successful. Experiments were successfully repeated on separate dates, as indicated in the manuscript.

Randomization

No specific randomization method was applied. Cultured cells were randomly allocated to treatment and control groups.

Blinding

Blinding was either not relevant or not possible to the study, because of the nature of the cell biology experiments using distinct cell lines and associated technical constraints.

Reporting for specific materials, systems and methods

We require information from authors about some types of materials, experimental systems and methods used in many studies. Here, indicate whether each material, system or method listed is relevant to your study. If you are not sure if a list item applies to your research, read the appropriate section before selecting a response.

Materials & experimental systems

n/a	Involved in the study
<input type="checkbox"/>	<input checked="" type="checkbox"/> Antibodies
<input type="checkbox"/>	<input checked="" type="checkbox"/> Eukaryotic cell lines
<input checked="" type="checkbox"/>	<input type="checkbox"/> Palaeontology and archaeology
<input checked="" type="checkbox"/>	<input type="checkbox"/> Animals and other organisms
<input checked="" type="checkbox"/>	<input type="checkbox"/> Clinical data
<input checked="" type="checkbox"/>	<input type="checkbox"/> Dual use research of concern
<input checked="" type="checkbox"/>	<input type="checkbox"/> Plants

Methods

n/a	Involved in the study
<input checked="" type="checkbox"/>	<input type="checkbox"/> ChIP-seq
<input checked="" type="checkbox"/>	<input type="checkbox"/> Flow cytometry
<input checked="" type="checkbox"/>	<input type="checkbox"/> MRI-based neuroimaging

Antibodies

Antibodies used

mouse anti-HA (for western blot: Sigma-Aldrich, H3663; for IF and IP: Sigma-Aldrich, HA-7, H9658), RanBPM (Bioacademia, 71-001, 5M; Santa Cruz Biotechnology, sc- 271727, F1), Vinculin (Cell Signaling Technology, E1E9V), SAP62 (Santa Cruz Biotechnology, sc-390444, A-3), Muskelin (Santa Cruz Biotechnology, sc-398956, C-12), ARMC8 (Santa Cruz Biotechnology, sc-365307, E-1), WDR26 (Abcam, ab85962), RMND5A (custom-made antibody from Yenzyme Antibodies), MAEA (R&D Systems, AF7288), DDX21 and DDX50 (Proteintech, 10358-1-AP, antibody recognizes both proteins, see supplemental figure 2), FLAG (SIGMA, F1804), HMGCS1 (Cell Signaling Technology, D1Q9D), and Actin (Cell Signaling Technology, 3700S). IF secondaries: Alexa 488 antibody against mouse (Invitrogen, Life Technologies, Cat # A32723), anti-mouse Alexa Fluor® 488 Conjugate (Cell Signalling Technologies; # 44085) and anti-rabbit Alexa Fluor® 594 Conjugate (Cell Signalling Technologies; #8889).

Validation

CTLH complex antibodies (RanBPM, MAEA, RMND5A, muskelin, WDR26, ARMC8) have been validated with knockdown or knockout experiments as per our previous publications (PMID: 31285494, 34383978). DDX21 and DDX50 knockdown experiments determined Proteintech 10358-1-AP antibody recognizes both DDX21 and DDX50 (Supplemental figure 2). All other antibodies used are highly cited that are shown on the product datasheet to recognize the target in human cell lines by western blot, producing a band at the expected molecular weight.

Eukaryotic cell lines

Policy information about [cell lines and Sex and Gender in Research](#)

Cell line source(s)

Flp-In™ T-Rex™ HeLa doxycycline-inducible cells were a kind gift from Dr. Arshad Desai's laboratory, San Diego, CA, USA. HEK293T cells were a kind gift from Sam Benchimol, York University (ATCC is original source). Wild-type HeLa and HEK293 cells were from ATCC. Cell line identity verification was done through STR.

Authentication

Cell lines were authenticated through morphology.

Mycoplasma contamination

All cell lines tested negative for mycoplasma as determined by MycoAlert Mycoplasma Detection kit (Lonza).

Commonly misidentified lines (See [ICLAC](#) register)

No commonly misidentified lines were used.

Plants

Seed stocks

Report on the source of all seed stocks or other plant material used. If applicable, state the seed stock centre and catalogue number. If plant specimens were collected from the field, describe the collection location, date and sampling procedures.

Novel plant genotypes

Describe the methods by which all novel plant genotypes were produced. This includes those generated by transgenic approaches, gene editing, chemical/radiation-based mutagenesis and hybridization. For transgenic lines, describe the transformation method, the number of independent lines analyzed and the generation upon which experiments were performed. For gene-edited lines, describe the editor used, the endogenous sequence targeted for editing, the targeting guide RNA sequence (if applicable) and how the editor was applied.

Authentication

Describe any authentication procedures for each seed stock used or novel genotype generated. Describe any experiments used to assess the effect of a mutation and, where applicable, how potential secondary effects (e.g. second site T-DNA insertions, mosaicism, off-target gene editing) were examined.